RSC Advances

PAPER

View Article Online
View Journal | View Issue

Cite this: *RSC Adv.*, 2025, **15**, 45822

Deep eutectic solvent-assisted chemosensing of Fe(III), V(III), C(II), and P(II) ions using a paper-based micro-array decorated by silver nanoparticles

Raana Tayefeh-Rahimian,[abc] Masoud Rismanchian,*[a] Mohammad Hasanzadeh *[b] and Arezoo Saadati[d]

Heavy metal pollution has become one of the most serious environmental and industrial challenges today. This is because of their toxicity, tendency to bioaccumulate in living organisms, and persistence in the environment. In recent years, various techniques have been developed to detect and quantify heavy metal contaminants. In this study, an innovative paper-based chemosensor (PCS) was constructed for the specific colorimetric recognition of Fe(III), V(III), Co(II), and Pd(II) ions in the presence of deep eutectic solvent (DES). This micro-array of PCS, mounted on fiberglass with a diameter of 5 mm for each zone of reaction. Thus, a miniaturized ion sensing substrate was proposed for low-cost, rapid, sensitive, and selective ion detection in real samples using a smartphone, with silver nanoparticles (AgNPrs) with a prism structure that serves as an optical probe. The DES-PCS combined with silver nanoparticles showed excellent performance in both semi-quantitative and quantitative analysis of Fe(III), V(III), Co(II), and Pd(II). Furthermore, an RGB-based absorbance method was used to estimate ion concentrations through digital image analysis with a color-picker app installed on a Samsung Galaxy A54 smartphone. High linearity was achieved for all analytes (R^2 > 0.975), with a low limit of quantification (LLOQ) ranging from 50 ng ml^{-1} to 1 μg ml^{-1}. The use of the developed DES-PCS confirmed that it is easy to detect Fe(III), V(III), Co(II), and Pd(II) in human biofluids, with results aligning well with those from standard solutions. Additionally, the DES-PCS demonstrated selective, sensitive, and stable responses without needing sample manipulation, making it suitable for on-site monitoring of ions in both occupational and environmental contexts.

Received 16th September 2025
Accepted 10th November 2025

DOI: 10.1039/d5ra07032e

rsc.li/rsc-advances

1 Introduction

Heavy metals are serious environmental hazards due to their toxicity, persistence, and bioaccumulation, and disrupt the body's metabolic functions. They can bind to vital cellular components and accumulate in organs like the liver, heart, kidneys, and brain, leading to diseases, organ failure, and an increased risk of cancer.[1–3] A burdensome metal-free environment is impossible; these metals enter the body through contaminated food, polluted water, and polluted air. Taking action to reduce exposure to heavy metals by effective detection, continuous monitoring, and remediation techniques is necessary to safeguard the environment and human health.[4] Therefore, developing simple methods for detecting metal particles is crucial to protect public health and the environment. Traditional techniques used for monitoring environmental contaminants, such as atomic absorption spectroscopy (AAS),[5] electrochemical methods,[6,7] inductively coupled plasma/atomic emission spectrometry (ICP/AES),[8,9] ICP mass spectrometry (ICP-MS),[10] and ultraviolet-visible (UV-vis) spectroscopy,[11] offer suitable sensitivity and accuracy even at low analyte levels. However, these methods require laboratory facilities, sophisticated and expensive instrumentation, and skilled operators, making them unsuitable for on-site environmental monitoring.[1] As a result, there is a growing demand for inexpensive, simple, sensitive, specific, portable, and cost-effective detection devices to overcome these challenges.

Paper-based analytical devices (PADs) are a point-of-use technology that have recently gained significant attention from both academic and industrial communities.[12,13] This interest comes from their simplicity, affordability, portability, and disposability.[14] These features offer real-world benefits across a wide range of applications where quick results and ease of use are essential. The importance of PADs lies in their ability to enable anyone, regardless of technical skill, to perform tests or monitor samples on-site, at the point of care. The PADs

[a]*Occupational Health Department, Isfahan University of Medical Sciences, Isfahan, Iran. E-mail: rismanchian@hlth.mui.ac.ir*

[b]*Pharmaceutical Analysis Research Center, Tabriz University of Medical Sciences, Tabriz, Iran*

[c]*Student Research Committee, Occupational Health Department, Isfahan University of Medicals Sciences, Isfahan, Iran. E-mail: hassanzadem@tbzmed.ac.ir*

[d]*Nutrition Research Center, Tabriz University of Medical Sciences, Tabriz, Iran*

concept is similar to the 'lab-on-a-chip' idea, but uses simple paper made from cellulose instead of a chip. Recently, PADs have become promising for heavy metal analysis because of their low cost, simplicity, portability, and ability to produce visible color changes upon analyte interaction.[15,16] This development opens new opportunities for applications in various research areas, including diagnostics, disease monitoring,[17,18] environmental monitoring,[19] food safety testing,,[20] and forensics.[21] Furthermore, paper-based sensing has been positively reviewed as an appealing platform that meets the World Health Organization's ASSURED criteria for an ideal rapid test, which are affordable, sensitive, specific, user-friendly, fast, robust, equipment-free, and easily accessible to end-users. This makes them an excellent option for reliable analysis in worldwide.[22] For better application, it is crucial to select an appropriate detection technique based on PADs analysis of different targets. Colorimetry, fluorescence, electrochemistry, and chemiluminescence are some of the most commonly used detection methods in PADs-based analysis. Each method differs in terms of sensitivity and the complexity of the required detection system, which affects its applicability for diverse applications.[23]

Colorimetric readouts are the most prevalent method of detection in PADs, enabling quantitative analysis of various samples, considering the philosophy of PADs (low-cost and user-friendly). Colorimetry is a commonly used method to generate signals in PADs because the analyte concentration can be directly correlated with the color intensity. While colorimetric systems are simple and effective, but have some drawbacks. A significant issue in quantitative colorimetric systems is the non-homogeneity of color across the test zones.[24] In PADs, colored indicators used for detection can migrate unevenly, leading to patchy color development (coffee ring effect). This happens because highly soluble signaling molecules spread outwards during the sample flow, accumulating at the edges of the designated detection zone. As a result, this can adversely affect the accuracy and precision of assays.[25,26] As a result, this can adversely affect the accuracy and precision of assays.

One significant limitation of colorimetric sensors is the shelf life of the samples and the stability of reagents in the test zone. This problem becomes apparent when the reaction responsible for the color change is very slow or requires prolonged contact between the analyte and the sensing reagents.[27] Consequently, solvent evaporation during the testing process can significantly restrict the application of these sensors for analysis and reduce their overall efficiency. Other significant challenge faced by colorimetric sensors is their performance in aqueous-phase analysis. For optimal results, the PADs or the indicators applied to the paper (the sensor elements) must be relatively hydrophobic. This hydrophobicity helps prevent undesirable color leaching and improves the uniformity of the results.[24] To overcome these limitations, the colorimetric indicator can be combined with a hydrophobic matrix that immobilizes on the paper surface.[28] Ionic liquids (ILs) have been proposed as alternative chemicals for fabricating various hydrophobic membranes.[29] However, ILs have some drawbacks. Such as needing complex multi-step synthetic procedures, involving prolonged reaction times at high temperatures, and necessitating the use of large quantities of chemical reagents and organic solvents, which can be harmful to the environment.[30] These drawbacks can be effectively overcome by utilizing solvents with low volatility, such as deep eutectic solvents (DESs).[31,32]

DESs have gained considerable attention as green and sustainable solvents since their introduction by Abbott *et al.* in 2003.[33] These solvents are created by combining two or more inexpensive components in specific molar ratios to form a eutectic system with a melting point that is significantly lower than that of the individual components.[34] Their popularity in the scientific community has grown significantly in the early years of this century as potential green alternatives to conventional solvents. This is due to their unique properties and advantages, including low vapor pressure at room temperature and the ability of their components to originate from biodegradable and/or renewable sources.[35–37] Additionally, their synthesis is inexpensive, typically straightforward, and allows for the preparation of solvents with the desired polarity, viscosity, and density.[38,39]

Among these, colorimetric detection using PADs is one of the most promising solutions. These devices work through specific reactions between target metal ions and optical probs or chromogenic reagents to produce detectable color changes that indicate the presence and amount of the analyte. In addition, PADs are not only affordable and easy to produce, but they also require minimal reagent use and are ideal for fieldwork and real-time environmental monitoring.[40,41]

Anisotropic metal nanoparticles have become notable because of their unique properties that can improve the performance of PADs. Among these, silver nanoparticles have received increasing attention in recent years due to their distinctive optical and chromogenic characteristics.[42] Previous studies show that T-AgNPrs have platelike triangular shapes with excellent electronic, optical, and structural properties.[43] Due to these traits, T-AgNPrs are especially important in developing paper-based colorimetric sensors. In metal nanoparticle-paper systems, ion binding can cause aggregation, etching, or surface deposition, which changes their plasmon resonance and thus their color. These mechanisms allow for rapid, selective, and quantifiable detection of analytes, with color changes visible to the eye or simple devices. Therefore, nanoparticles have proven essential in creating various PADs.[40,41] Although they offer many advantages, challenges such as nanoparticle aggregation and instability over time remain; in this regard, using eutectic liquids could help broaden their applications. Thus, we examine a new approach combining DESs and silver nanoparticles with a PADs to improve analytical performance and support environmental sustainability.[43]

Modern smartphones, equipped with high-resolution cameras and advanced image processing capabilities, enable precise quantification of colorimetric responses, making them ideal for portable analysis. The integration of smartphone-based detection with PADs seamlessly merges qualitative and quantitative analysis, greatly enhancing their capabilities and transforming them into portable, user-friendly diagnostic tools that are ideal.[44,45] As a result, the versatility of PADs-based

sensors has broadened, allowing for their effective application across various matrices, including water, soil, food, and biological fluids.[46,47] Studies have successfully demonstrated the application of paper-based colorimetric sensors (PCS) for detecting heavy metals such as chromium, lead, cobalt, cadmium, and mercury.[46,48–50] Based on these features and at continuing our previous report,[51] this study presents a novel approach for on-site detection of Fe^{3+}, V^{3+}, Co^{2+}, and Pd^{2+} ions by integrating a DES with a PADs decorated by T-AgNPrs. To achieve this, the reaction of the analyte with T-AgNPrs in the presence of DES (DES/ion-T-AgNPrs) was employed to produce a colored product on the PADs. The choice of a hydrophilic DES as the reaction medium was initially made, and its performance was compared to that in the ion-AgNPrs medium, which is traditionally used. Then, the proposed DES-PCS, with silver nanoprisms as an optical probe, was used to quantify the ion levels of Fe^{3+}, V^{3+}, Co^{2+}, and Pd^{2+} through smartphone-based absorbance measurements. Smartphone-based colorimetric analysis provides quantitative results within one minute, offering a rapid and cost-effective alternative to conventional methods. This work represents a significant advancement in PCS technology, addressing critical limitations of existing platforms while maintaining simplicity and affordability. This colorimetric device, tested in human urine samples, validated the performance for cation detection under optimal conditions (see Scheme 1).

2 Experimental section

2.1 Materials and apparatus

Silver nitrate ($AgNO_3$, ≥99.8%), polyvinylpyrrolidone (PVP) K-30, sodium borohydride (NaBH4, ≥96%), trisodium citrate (≥99%), and hydrogen peroxide (H_2O_2, 30 wt%) were acquired from Sigma Aldrich (Ontario, Canada). Choline chloride (ChCl, >98%) and ethylene glycol (EG, >98%) were purchased from Merck Chemicals Darmstadt, Germany. The metal ions (As^{3+}, B^{3+}, Fe^{3+}, Ca^{2+}, Te^{4+}, V^{3+}, Sr^{2+}, W^{6+}, Co^{2+}, Zr^{4+}, Na^{+}, Mo^{6+}, Al^{3+}, Ba^{2+}, Cr^{3+}, Pt^{4+}, Bi^{3+}, Sn^{2+}, Mn^{2+}, Pb^{2+}, Ni^{2+}, Cs^{+}, Si^{4+}, Hg^{2+}, Se^{4+}, K^{+}, Li^{+}, Zn^{2+}, Mg^{2+}, Pd^{2+}, and Cu^{2+}) Stock solutions of 1 μg ml^{-1} were prepared from chemlab company (Zedelgem, Belgium). Glass fiber papers (55 mm) were supplied from Schleicher & Schuell GmbH, Germany (ref. no. 10 370 55 and lot no. FL 091-1) and solid paraffin was acquired from the local commercial shop in Tabriz, Iran. Deionized water was provided by Ghazi Pharmaceutical Company, Tabriz, Iran.

2.2 Instruments

Ultraviolet-visible (UV-vis) spectrophotometer (A Shimadzu UV-1800) with a one-nanometer resolution using a quartz cell. The reaction solutions were scanned at a wavelength of 200–800 nm. The size distribution and zeta potential of the formed silver nanoprisms were characterized using a ZetaSizer Ver. 7.11 (Malvern Instruments Ltd, MAL1032660, England). The Fourier-transform infrared (FT-IR) spectra were recorded in the range of 500–4000 cm^{-1} by a Thermo Fisher FT-IR spectrophotometer. During the experiments, all of the digital photos and videos of PCSs were captured using a Samsung Galaxy A54 smartphone with a 13 Mpx camera.

2.3 Syntheses and characterization of triangular silver nanoprisms (T-AgNPrs)

T-AgNPrs were successfully synthesized by reducing silver nitrate in an aqueous solution with sodium borohydride as

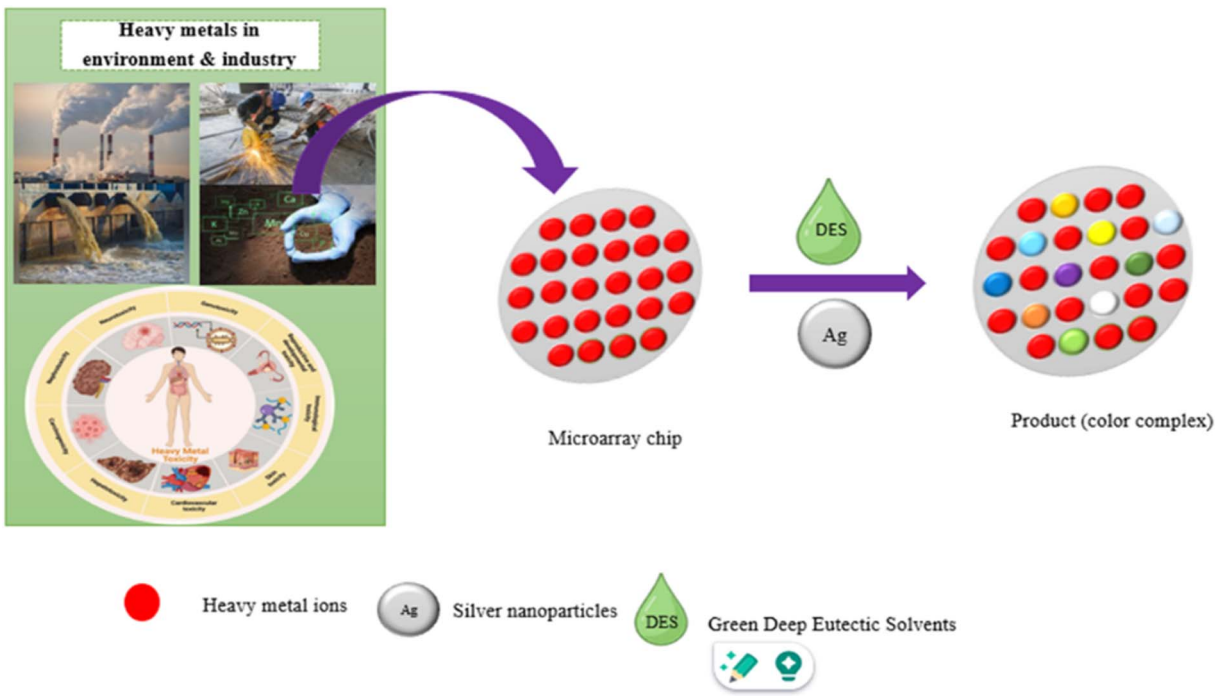

Scheme 1 PCSs-based analysis of Fe(III), V(III), Co(II), and Pd(II) ions using DESs-assisted chemosensing.

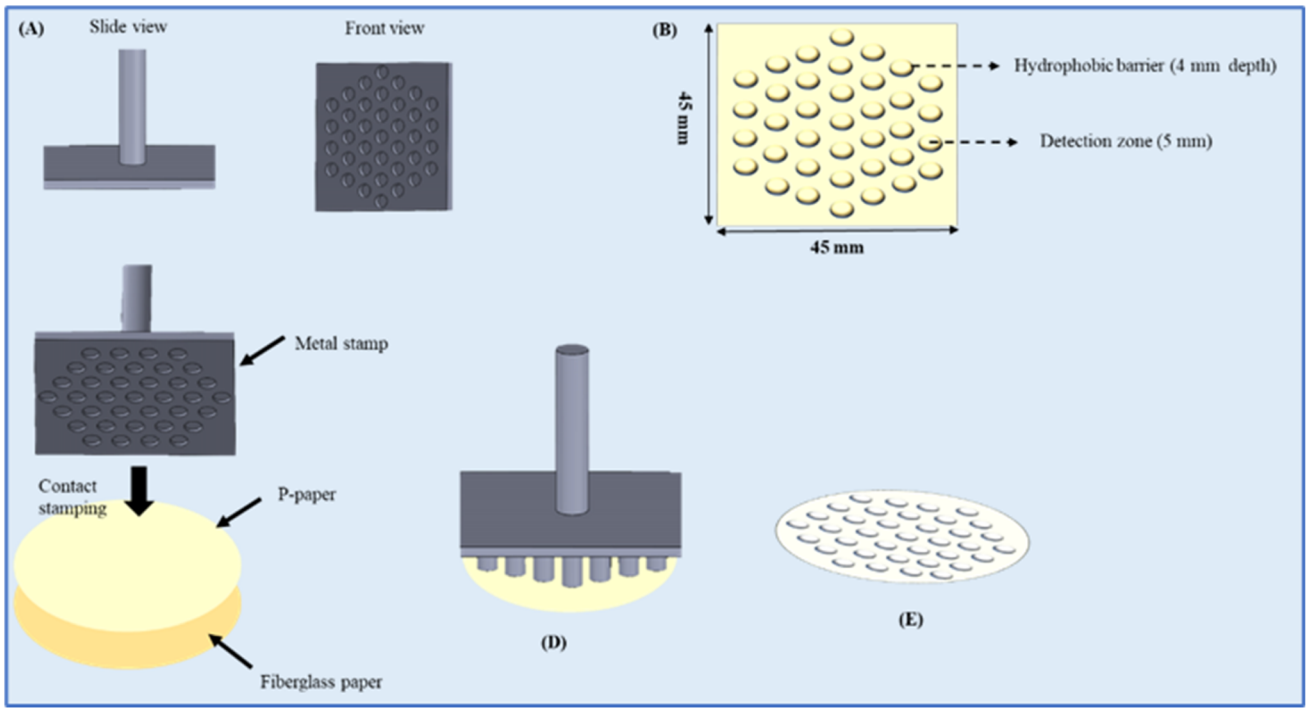

Scheme 2 Fabrication steps for the microarray PCS by contact stamping. (A) Photograph of the custom-designed stamping device, (B) stamping pattern of the hydrophobic barrier and semi-hydrophobic detection zone, (C) a paraffinized paper (p-paper) is placed over the native fiberglass paper (n-paper) surface, (D) the metal stamp is heated to 180 °C and pressed into contact for 20 seconds, (E) represents a typical microarray PCS fabricated by the proposed method.

a strong reducing agent at room temperature and characterized using UV-vis absorption spectroscopy, DLS, TEM, and FE-SEM, as previously described in our earlier report.[52]

2.4 Synthesis and characterization of DES

The hydrophilic DES was synthesized by mixing choline chloride as an HBA (hydrogen bond acceptor) with ethylene glycol and as an HBD (hydrogen bond donor) in a 1 : 2 molar ratio. This hydrophilic DES was chosen because it is fast and easy to synthesize, and it has a low viscosity (37 cP at 25 °C), which facilitates the analysis.[51]

2.5 Fabrication of the microarray of PCS

Design and fabrication are crucial for producing accurate colorimetric results with micro-scale samples using paper-based microfluidic devices. In this work, PCS were fabricated using a stamping-based method that our group recently introduced due to its simplicity.[52] Initially, the PCS patterns were designed with Catia software, featuring a petal-like shape and a 32-array pattern with dimensions of 45 mm × 45 mm. To start, paraffin was heated until liquid, and the fiberglass paper was immersed in the liquid paraffin at 90 °C for 60 seconds. Afterward, the paraffinized paper was removed and allowed to cool at room temperature. The paraffin-coated paper was then placed on the surface of the original fiberglass paper, and both were pressed together using a strong magnet and a metallic stamp. The metal stamp, containing the microfluidic network, was preheated to 180 °C (optimized temperature) on a hot plate for 20 seconds (optimized time) and then pressed against the paraffin-coated paper for 15 seconds. Through simultaneous heating and pressing, the original paper developed hydrophobic and semi-hydrophobic areas as designed by the paraffin. After drying, the prepared PCS was used for colorimetric analysis. In this study, two different PCS were created using fiberglass paper: (1) an eight-zone circular layout surrounding a central zone for metal ion detection and specificity testing. All channels in this device were approximately 10 mm long and 3 mm wide, with detection zones measuring 5 mm in diameter and the central zone 10 mm. (2) A 32-zone array, designed specifically to test detection limits, with each zone having a diameter of 5 mm (Scheme 2).

After conducting our analysis, we established that an optimized depth of 500 micrometers was ideal for the metal template used in fabricating the PCS. The assay results indicated that the detection zones had better resolution on the microscale substrate prepared with a depth of 500 micrometers. The formation of hydrophobic detection regions was validated. The solution diffuses in a radial direction from the center of the area to the periphery. The diffusion stops when the liquid hits the wax boundary. This confirms the boundary on all sides of the detection zones.

2.6 Assay protocol

After fabrication of the PCS, colorimetric detection of candidate metal ions was carried out using the DES-PCS designed with

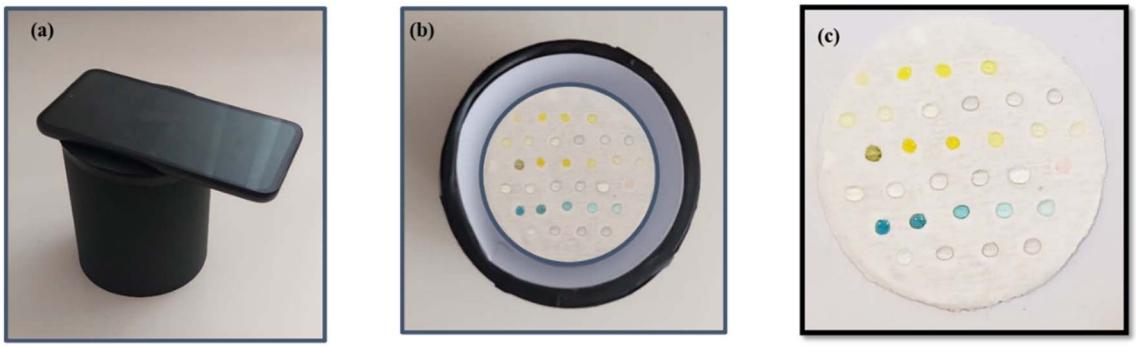

Scheme 3 Cylindrical box format designed for capturing digital images: (a) a handmade box with an A54 smartphone placed on top, fixed at a height of 110 cm; (b) the bottom part of the box with the microarray test fixed for image acquisition, (c) microarray paper that contains the colored product, with concentrations ranging from 1 ng ml^{-1} to 1 μg ml^{-1}.

a petal pattern. To assess the colorimetric responses, 5 μL solutions of Fe(III), V(III), Co(II), and Pd(II) metal ions were pipetted onto the PCS. Then, 5 μL of DES and AgNPrs probes were added to the detection zone, respectively. A total of 15 μL of the sample was placed in the center of the detection zone, and the PCSs were left at room temperature until the reaction was complete. Additionally, heavy metal ion solutions at various concentrations were analyzed using spot PCSs to determine each metal ion's detection limit. For each metal ion, ten solutions with concentrations ranging from 1 ng ml^{-1} to 1 μg ml^{-1} were prepared and spotted onto PCS, arranged in a 36-zone array. After the reactions concluded, the color changes were recorded visually and through photographs. The handheld device was carefully assembled to optimize sensitivity, with particular attention paid to the distance between the sample and the smartphone camera used for image capture, as well as

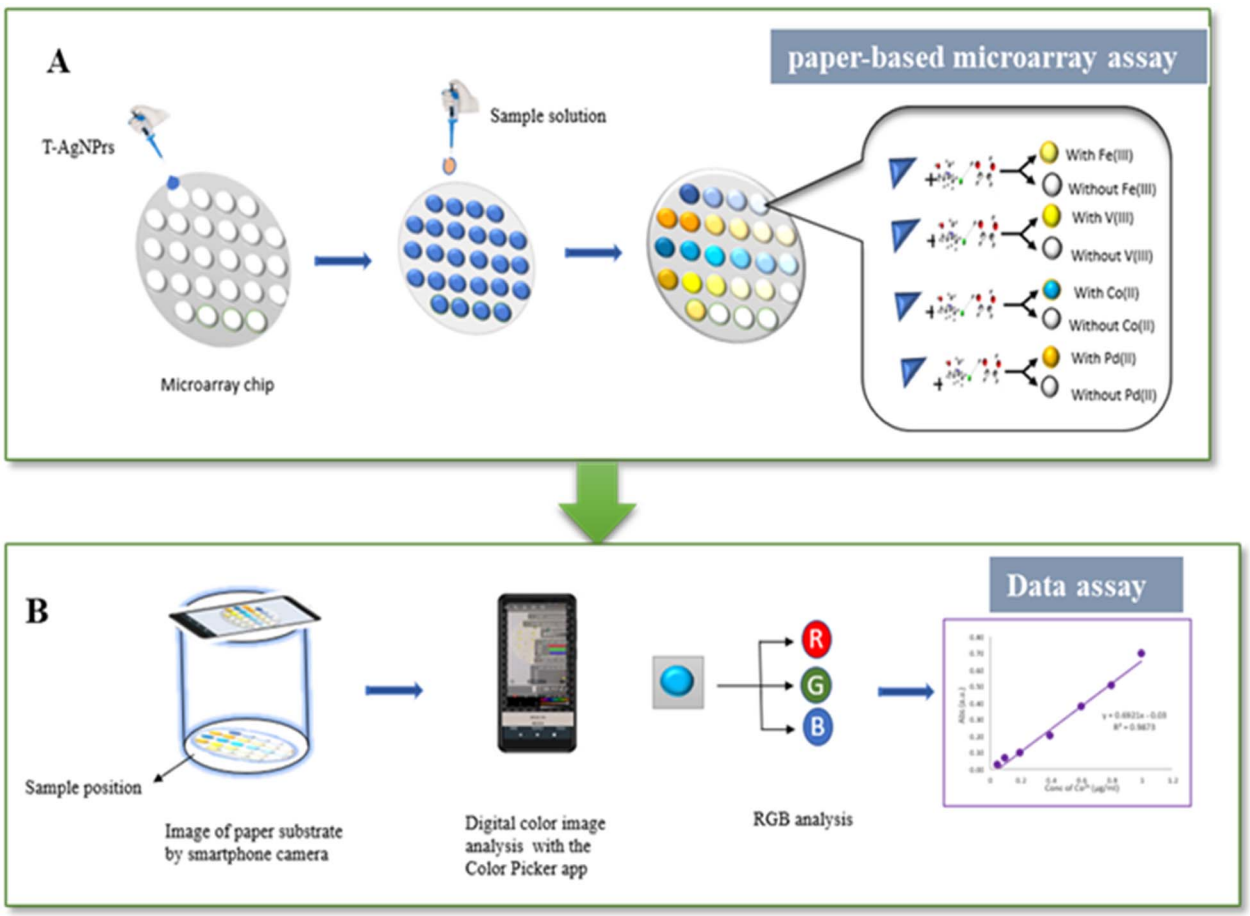

Scheme 4 (A) Illustration of the colorimetric paper-based microarrays fabricated on fiberglass for the simultaneous detection of multiple metal ions (Fe(III), V(III), Co(II), and Pd(II)). (B) The design of a smartphone-based portable reader with an app to acquire colorimetric changes from the microarray and report the results.

to the camera's positioning to ensure proper focus. After optimizing these parameters, a distance of 10 cm was maintained between the paper array of the PCS and the smartphone to achieve excellent results. Subsequently, the DES/ion-T-AgNPrs spots on PCS with different concentrations were subjected to absorbance measurements. Multiple photos were taken of each paper, and the RGB values and wavelengths were analyzed using a color picker app. To control luminosity and prevent interference from external light sources, the color images were captured using a homemade device cylindrical box 110 cm tall with an inner diameter of 10 cm. The inside of the box was lined with white polymer to better capture color changes and reduce reflections from the light source in the smartphone images. A hole at the top of the box aligned with the camera lens (8 MP) of a smartphone positioned about 110 cm above the paper tests, and the images were taken using autofocus with the flash as the light source. After optimizing these parameters, a 110 cm distance between the paper array and the smartphone was maintained to get the best results (Scheme 3). Multiple photos were taken for each paper, and a smartphone color picker app (**https://gmikhail.github.io**, version 7.4.2)-based on red–green–blue (RGB) analysis-was used to evaluate the color intensity of four candidate metal ions. This powerful, free software provides immediate RGB values and color names directly on the screen, without additional digital image processing or transformations. It also allows adjusting the size of the focused color area from which RGB values are collected. These values were used to create calibration plots and to detect ion concentrations in real samples. To ensure consistent data, all images were captured at 5, 30, 60, 90, and 120 minutes after the start of the reaction.

2.7 Absorbance measurement using the digital image analysis

The smartphone camera was placed above the optical window of the enclosure to capture high-resolution images (4096 pixels) of the colorimetric responses on the PCSs. A specialized color picker application was utilized to extract the RGB (red–green–blue) values and the dominant wavelength from the images (Scheme 4).

The zone (RGB) with the highest color intensity was selected for each analyte to calculate RGB-based absorbance, also known as colorimetric absorbance. The RGB values obtained from the image directly correspond to the light intensity entering the camera detector. Therefore, the negative logarithm of the relative recorded intensities of the RGB zones indicates the "colorimetric absorbance" value, as shown in the equation, $A_{RGB} = -\log(RGB/R_0G_0B_0)$, where A_{RGB} is the colorimetric absorbance, RGB indicates the actual color values of the sample, and $R_0G_0B_0$ are blank values in the absence of the target, based on the Beer–Lambert equation. Therefore, the colorimetric absorbance value obtained is proportional to the concentration of the dye, in accordance with Beer's law.[53] This method is recommended for quantitative analysis because it effectively compensates for variations in background lighting conditions. These values were used to create calibration plots between absorbance (A) and the concentration of the solution in the linear range of 1 ng ml^{-1} to 1 μg ml^{-1}. The analysis was performed on all experiments repeated in triplicate. Preliminary tests were conducted to improve performance, selectivity, and stability, including the order of adding materials (ion, probe, and DES), DES type, reaction time, stability time, and paper type (polyurethane, TLS, filter paper, and glass fiber paper).

In summary, the physical adsorption and vaporization of molecules on PCS often lead to reduced activity, poor uniformity, heterogeneity in colorimetric analysis, and disruptions in quantitative measurements. Additionally, the use of the DES showed a stable and uniform color distribution on PCSs. Therefore, a PCS incorporating DES can serve as a sensitive tool for detecting heavy metals. The DES-PCS does not rely on expensive instruments, and its simple operation allows non-experts to perform the analysis.

2.8 Real sample analysis

The validity of the prepared PCSs for detecting Fe(III), V(III), Co(II), and Pd(II) ions in real samples was assessed by the colorimetric analysis method. Human urine was spiked with precise concentrations of candidate metal ions to validate the DES-PCS method capabilities for their detection in a real sample. For this purpose, a 5 μL solution with T-AgNPrs was dropped on the detection zone of the PCS and allowed sufficient time for a complete reaction. The resultant color changes on the PCSs were analyzed and compared to standard solutions, ensuring the accuracy of the suggested method. Human urine samples were obtained from Tabriz University of Medical science, Tabriz, Iran, (ethic code: IR.TBZMED.REC.1404.260). All experiments were performed in accordance with the guidelines of institute (Tabriz University of Medical science), and approved by the ethics committee at Tabriz University of Medical science, Tabriz, Iran. Informed consents were obtained from human participants of this study.

3 Results and discussion

3.1 DES-induced T-AgNPrs aggregation

Upon addition of deep eutectic solvent (DES) to T-AgNPrs, a rapid color change from bright blue to colorless is observed. This phenomenon is primarily due to aggregation of the triangular silver nanoprisms. Dynamic light scattering (DLS) measurements confirm that the hydrodynamic diameter increases from 20.4 nm to 931.8 nm, while zeta potential shifts from −15 mV to near-neutral values (0.613 mV). This near-neutralization of surface charge destabilizes the colloid, causing the characteristic localized surface plasmon resonance (SPR) peak of the nanoprisms to diminish, resulting in loss of color.

Importantly, this DES-induced aggregation is a physical process and does not involve chemical reaction with analytes. Subsequent colorimetric responses upon addition of metal ions (*e.g.*, Ag^+, Cu^{2+}) are mediated by the T-AgNPrs and not by DES alone. Control experiments demonstrate that in the absence of T-AgNPrs, DES solutions containing analytes show negligible color changes, confirming the central role of the nanoprisms in

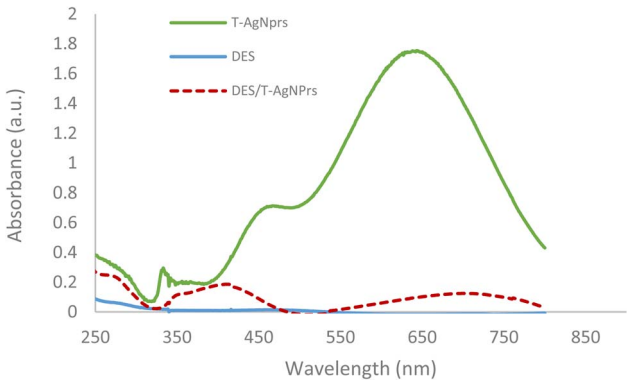

Fig. 1 UV-vis spectra of the T-AgNPrs and T-AgNPrs/DES with the maximum wavelength of selective reflection corresponding to T-AgNPrs and T-AgNPrs/DES.

sensing. Thus, DES acts primarily as a stabilizer and aggregation inducer, providing a controlled environment in which T-AgNPrs can selectively interact with target analytes to produce measurable color changes (Fig. 1).

The DES, composed of ethylene glycol and choline chloride, possesses unique properties due to its components. Choline chloride has both positive and negative charges, allowing its chlorine atoms to form hydrogen bonds with hydrogen atoms in ethylene glycol. Notably, no chemical reactions occur between the DES and T-AgNPrs; instead, two main forces define their structure. The first is electrostatic attraction, where the negatively charged citrate groups on T-AgNPrs are drawn to the positively charged choline chloride in the DES. The second involves hydrogen bonding, with chlorine and nitrogen atoms in the DES bonding to the free hydroxyl groups on the T-AgNPrs surface. This combination of forces demonstrates the effectiveness of using DES in this context, showcasing its potential benefits. The electrostatic and hydrogen bonding forces create a network that significantly increases the flexibility of T-AgNPrs with a DES. As a result, DES-T-AgNPrs exhibit exceptional optical and detection capabilities in this study. In conclusion, analysis of UV-vis spectroscopy, zeta potential, and particle size tests suggests that T-AgNPrs in the DES are in a state of self-aggregation. This aggregation is attributed to the properties of the DES, as well as the physical interactions between the T-AgNPrs and the DES.

3.2 Optimization and enhancement of detecting parameters of DES-PADs

To achieve higher performance, such as sensitivity and stability, this section discusses the impact of various variables, including the type of substrate, amount of sample, type of DES, order of adding materials to the surface of PCSs, and reaction time, that were investigated.

3.2.1 Type of paper. In the fabrication of PCSs, hydrophilic capillary zones or spots are created on the surface of paper using hydrophobic materials, with no chemical reaction occurring between cellulose and the hydrophobic substances. Therefore, choosing the appropriate type of paper is crucial, considering factors such as resistance to decomposition and deformation, absorption capacity, thickness, wicking rate, porosity, homogeneity, and color intensity. Understanding these factors is essential for the selection of substrates to fabricate appropriate PCSs tailored for a specific reaction system.[54] The selection process should not be random; it must consider paper properties such as thickness, porosity, wicking rate, and bulk. These factors are crucial to ensure that they meet the requirements of the reaction, including the interactions between analytes/reagents and the cellulose fiber network, the sample volume, and analyte/reagent mobility. This careful selection will help produce optimal color results.

For effective colorimetric analysis on PCSs, the paper substrates must be white and free of discoloration, which can occur during prolonged storage.[55] Additionally, the complex formed between the metal and optical probe must be evenly distributed across the detection zone to enhance accuracy and precision. Consequently, choosing the most suitable paper for each task is essential. In this study, Whatman filter papers no. 42, polyurethane, TLC, office paper, parafilm, and fiberglass were evaluated for colorimetric analysis of ions using PCS. Due to the small pore sizes of Whatman no. 42, samples were absorbed quickly, making it difficult to observe any color changes. The heat from the stamp deformed the polyurethane during fabrication, and the colored complex moved on the parafilm. Therefore, in this research work, fiberglass paper was utilized to fabricate PCSs.

3.2.2 Optimization of volume sample. An injected volume on the PCS affects the quantity and color intensity of the sensor. To determine the optimal volume of optical probe, T-AgNPrs was used due to its intense blue color, which facilitates clear and naked-eye visualization. Sample volumes between 5 and 20 μL were tested. Volumes less than 10 μL did not adequately cover the detection area, while volumes greater than 15 μL overflowed beyond the designated zone. Among all the volumes tested, 15 μL was determined to be optimal, as it provided sufficient coverage without any overflow. This volume was used in subsequent experiments.

3.2.3 Selection of DES. An essential parameter in this assay is the type of DES used to attach the PCSs for the optical sensing of metal ions, maximizing the interaction between silver nanoparticles (probe) and the sample (analyte). Table S1 (SI) summarizes the hydrophilic DESs that were synthesized with various hydrogen bonding donors (HBDs), hydrogen bonding acceptors (HBAs), and molar ratios. DES-PCSs with different DES compositions (ChCl/EG, ChCl/glycerol, and ChCl/urea) were prepared and tested for ion sensing using PCSs. The assay results show that no significant color changes occurred for metal ions in the presence of ChCl/urea (DES3) solvent. Among the two solvents, DES1 and DES2, designated as solvent 1 and solvent 2, both successfully detected Fe(III), V(II), Co(II), and Pd(II) by PCSs. However, due to the higher viscosity of DES2, the reaction time of the analyte and probe was longer compared to DES1. Based on these findings, DES1 (ChCl/EG) was selected for the next steps of the experiment.

3.2.4 Order of adding materials on paper. The sequence in which the DES, T-AgNPrs probe, and ion target were added to

Table 1 Order of adding material on paper sensors for detection (III), V(III), Co(II), Pd(II)

Order of adding material	Fe(III)	V(III)	Co(II)	Pd(II)
Ion + DES + T-AgNPrs				
Ion + T-AgNPrs + DES				

the PCSs was also examined. As shown in Table 1, whether an equimolar ion was added before or after the addition of T-AgNPrs to the DES, the color intensities remained consistent. This indicates that the order of adding DES and the ion did not affect the final signal.

3.2.5 Response time. The response time refers to how long it takes for the DES-based PCS to show a visible color complex when exposed to the metal ion solution. Optimization involves determining the point at which the color change is stable and easily distinguishable. Factors such as paper porosity, reagent diffusion, and ambient conditions can influence the response time. The RGB-based absorbance at various time intervals was measured for Fe(III), V(II), Co(II), and Pd(II). This monitoring indicated that the reaction had reached completion, as no significant color change occurred afterward. To ensure a complete reaction and due to the high stability of the immobilized indicators, the DES-PCS was monitored for 2 hours. The results of this response time study are presented in Fig. 2. This parameter is essential for practical applications, as a quicker response time is preferred for rapid testing.

Extended incubation periods longer than 60 minutes resulted in the diffusion of the optical sensor (T-AgNPrs); however, vaporization was effectively prevented due to the presence of DES. The time needed for visible changes in the color of the immobilized indicators for each of the ions varied in the presence of DES. This parameter is crucial for practical applications, as a quicker response time is preferred for rapid testing. However, this study indicates that the response time of DES-PCS to metal ion solutions is relatively slow due to the viscosity of the DES.

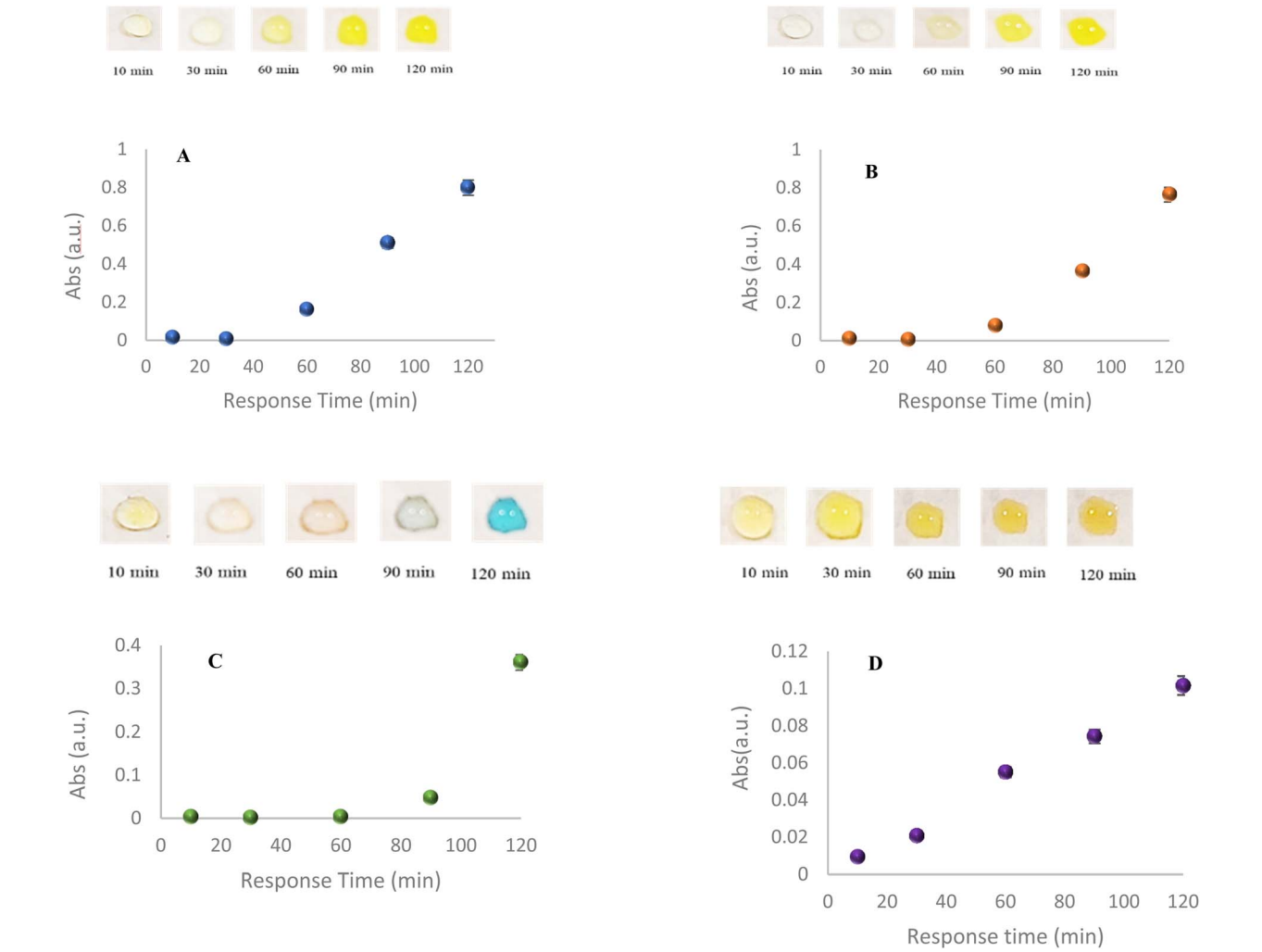

Fig. 2 Response time of PCSs (A)Fe(III), (B)V(II), (C) Co(II), and (D) Pd(II) ions in the presence of DES.

Table 2 The obtained color and RGB color codes on the DES-PCS after complete reaction of the Fe^{3+}, V^{3+}, Co^{2+}, and Pd^{2+} ions and T-AgNPrs

Metal ion	Fe(III)	V(III)	Co(II)	Pd(II)
Color name	Dandelion yellow	Greenish yellow	Middle blue	Metallic gold[a]
Hex color code[a]	E8DA37	EFED67	EFE8DB	D9B564
RGB color code	RGB (232, 218, 55)	RGB (239, 237, 103)	RGB (239, 232, 219)	RGB (217, 181, 100)
CMYK values[a]	0.0%, 6.0%, 76.3%, 9.0%	0.0%, 0.8%, 56.9%, 6.3%	0.0%, 2.9%, 8.4%, 6.3%	0.0%, 16.6%, 53.9%, 14.9%

[a] Color-hex gives information about colors, including color models. CMYK values are a combination of cyan, magenta, yellow, and black.

3.3 Chemosensing of Fe(III), V(III), Co(II), and Pd^{2+}(II) ions using PCS in the presence of DES

After optimization of experimental conditions, PCSs were utilized for the simultaneous analysis of four metal ions: Fe^{3+}, V^{3+}, Co^{2+}, and Pd^{2+} with silver nanoparticles in the presence of DES. For colorimetric analysis, the detection zone was prepared by adding 5 μL of standard solutions of Fe^{3+}, V^{3+}, Co^{2+}, and Pd^{2+} at a concentration of 1 μg ml^{-1}. Then, DES and freshly prepared T-AgNPrs, in a 1 : 1 ratio v/v (5 μL each), were added to the detection zone, where formed a color complex. The detection mechanism harnesses the power of T-AgNPrs aggregated in a DES to deliver precise results. Specifically, T-AgNPrs interact with Fe^{3+}, V^{3+}, Co^{2+}, and Pd^{2+} ions on the surface of PCSs, resulting in vibrant color complexes: dandelion yellow for Fe^{3+}, greenish yellow for V^{3+}, middle blue for Co^{2+}, and metallic gold for Pd^{2+}. This effective approach not only ensures accurate detection but also enhances visual confirmation in the test zone. This visible color change can be easily seen with the naked eye on the PCS. The color intensity of the generated complex was evaluated using a smartphone equipped with software. Observations made with the naked-eye, along with the detection of color intensity, indicated that both detection methods showed significant results in the presence of DES. It was concluded that these ions formed a stable-colored complex with silver nanoparticles in the presence of DES(DES/ion-T-AgNPrs).

We have conducted control experiments using Ag^{+} ions in DES without T-AgNPrs. These experiments showed that the colorimetric response in the absence of nanoprisms is negligible compared to the DES/AgNPrs system, confirming that the observed color changes are mediated by T-AgNPrs interactions with analytes in the DES matrix.

In addition, the results show that the reaction between metal ions and T-AgNPrs can occur in ChCl-EG at room temperature,

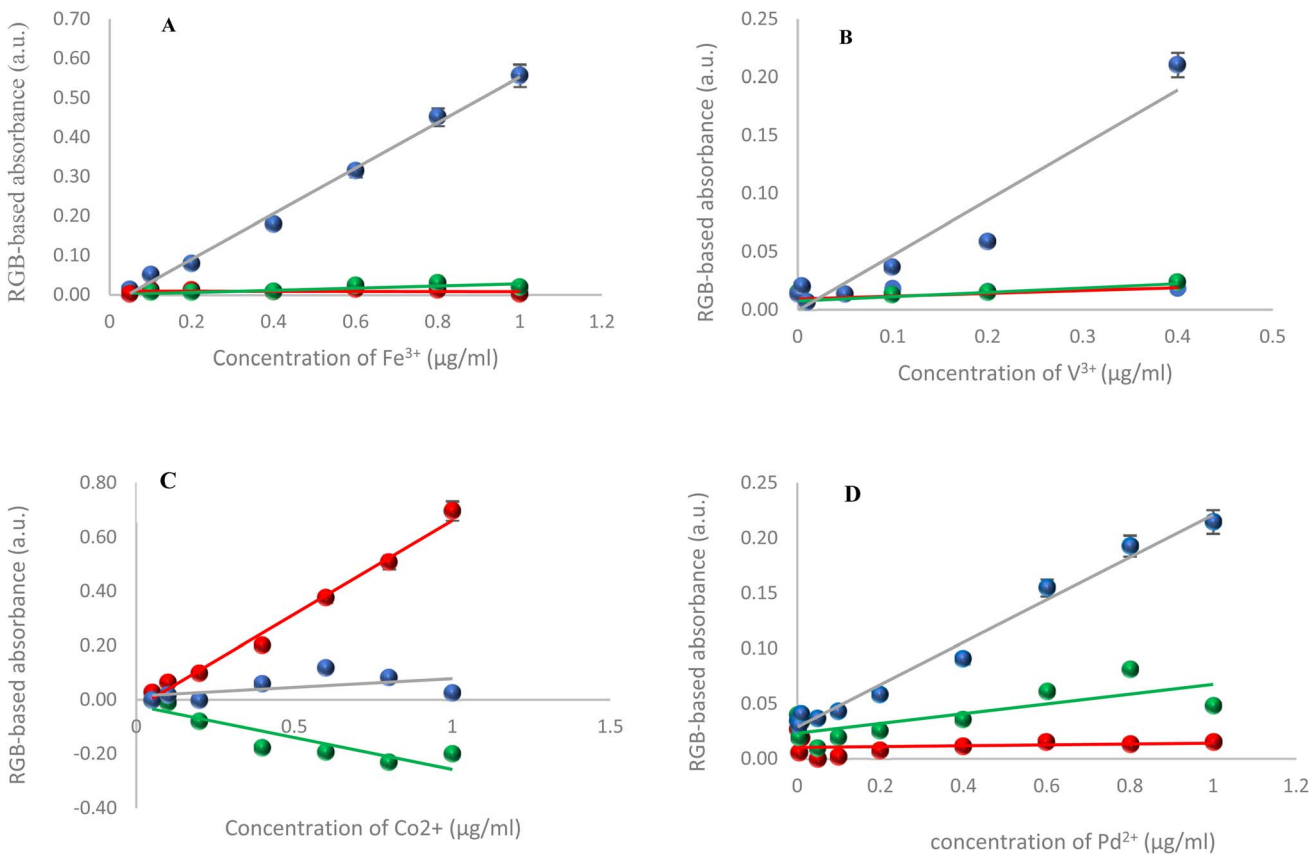

Fig. 3 RGB values of the color complex formed between metal ions and PCS decorated by DES-T-AgNPrs, (A) Fe(III), (B) V(III), (C) Co(II), and (D) Pd(II).

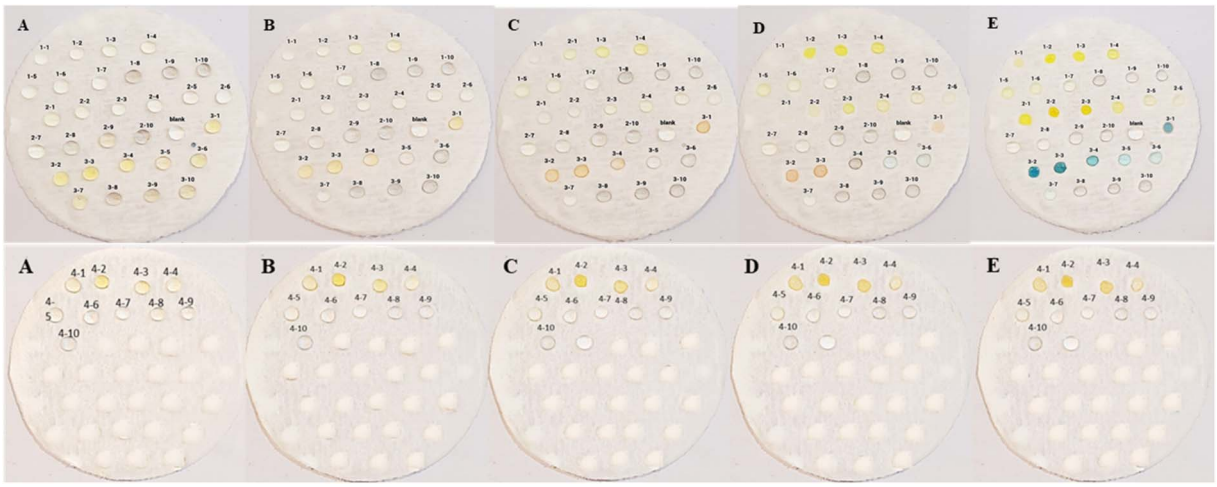

Fig. 4 Digital photos of DES-PCS decorated with T-AgNPrs and samples standard with varying concentrations of metal ions: (1) Fe^{3+}, (2) V^{3+}, (3) Cd^{2+}, and (4) Pd^{2+} injected into sensing zones at different reaction times (A) after 5, (B) 30, (C) 60, (D) 90, and (E) 120 minutes. The concentrations for each metal ion were as follows: (1) 1 μg ml^{-1}, (2) 0.8 μg ml^{-1}, (3) 0.6 μg ml^{-1}, (4) 0.4 μg ml^{-1}, (5) 0.2 μg ml^{-1}, (6) 0.1 μg ml^{-1}, (7) 50 ng ml^{-1}, (8) 10 ng ml^{-1}, (9) 5 ng ml^{-1}, and (10) 1 ng ml^{-1}, all of which were used at a 1 : 1 v/v ratio.

albeit very slowly due to the high viscosity of the DES. This slow reaction rate provides sufficient time for analyte molecules to interact with the nanoparticle surfaces, thereby overcoming mass transport limitations and enhancing the sensitivity and selectivity of colorimetric PCSs. Moreover, the gradual reaction time does not greatly limit the application of DES in the micro-scale zone of PCS, especially considering the exceptionally low vapor pressure of DES at room temperature. Although the color change may require some time, its stability over several days without drying makes it a highly reliable option.

Notably, the colorimetric analysis demonstrated that the use of the DES revealed a stable and homogenous color distribution on PCSs. Therefore, this highlights the significant benefits of using DES for improved detection of metal ions by PCSs (Table 2).

The concentrations of Fe^{3+}, V^{3+}, Co^{2+}, and Pd^{2+} were effectively determined using RGB values extracted from images, as illustrated in Fig. 3. Regression analysis revealed that the red channel was highly effective for detecting Co(II). In contrast, the blue channel exhibited remarkable linearity and exceptional sensitivity for detecting Fe(III) and V(III). These findings support the use of the red channel for the precise quantitative analysis of Co(II), while the blue channel is employed for accurate detection of Fe(III) and V(III).

3.4 Analytical performance

For accurate and sensitive analysis, solutions with known concentrations of Fe(III), V(III), Co(II), and Pd(II) were determined using the proposed PCS (32-array format). Calibration graphs plotting the absorbance of the sensor against concentrations of candidate metal ions to assess the analytical performance of PCS in the presence of the DES. First, standard ion solutions in DES at various concentrations ranging from 1 ng ml^{-1} to 1 μg ml^{-1} were introduced into the sample detection zone of the PCSs, arranged from the highest to the lowest concentration. Next, 5 μL of T-AgNPrs was immediately dispensed onto the detection zone of the PCS, which already had 5 μL volume of ion solutions loaded. The detection zone was visually monitored within 120 min to ensure the formation of the T-AgNPrs-ion complex on the DES-PCSs (Fig. 4).

The PCS system showed accurate responses to different concentrations of analytes, producing distinct reactions compared to the blank. The metal ions interacted with the optical probe, leading to the formation of colored metal complexes in the sensing zones. Samples with higher concentrations gave higher intensity readings, and less intense coloring was observed for shorter exposure times. The colored metal complexes on PCS were then measured using colorimetric absorbance with the homemade instrumentation described in Section 2.4 to evaluate the device's performance and confirm whether the observed colors correlate with ion concentration in the samples. Calibration curves for each species were plotted using absorbance derived from the RGB model against varying concentrations of analytes (Fig. 8). The RGB-based absorbance measurements for blank and each of candidate ions were done by smartphone (Samsung A54) for the red (R), green (G), and blue (B) channels using $A = -\log[I/I_0]$ as described in ref. 42 and 43; where I = RGB values of the (DES/T-AgNPrs-ion) sample, and I_0 = RGB values of the blank on the PCS. The calibration samples were analyzed in triplicate.

In the initial minutes of the reaction, all Fe^{3+} concentrations appeared colorless. However, as the reaction progressed, higher concentrations of Fe^{3+} (1, 0.8, 0.6, 0.4, 0.2, 0.1 μg ml^{-1}, and 50 ng ml^{-1}) gradually changed to a yellow color after approximately 90 minutes (the optimized incubation time). In Fig. 5A, the values increased as the target concentrations increased, then the values gradually reached a steady state at an analysis concentration of 50 ng ml^{-1}, which corresponded, by visual inspection, to images of patterned PCS of low color intensity. Comparing the correlation between color change and the amount of Fe^{3+}, the color of the PCS changed from dark yellow to light yellow when the concentration of Fe^{3+} decreased (see

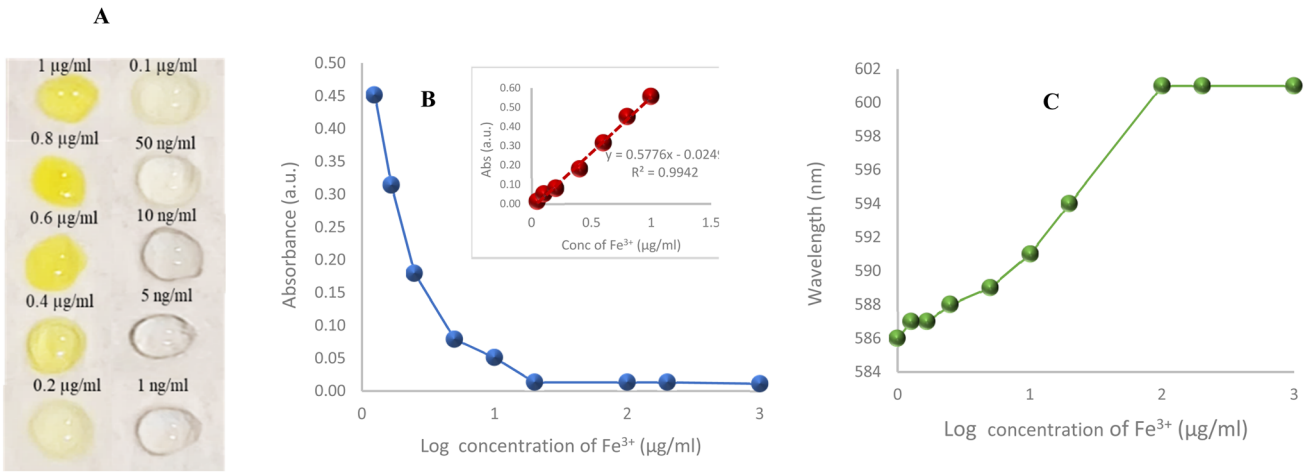

Fig. 5 Colorimetric results for Fe^{3+} determination using DES-PCS. (A) Images for the PCS displayed different Fe^{3+} amounts. (B) The calibration curve indicated the correlation between the value of RGB-based absorbance and the concentration of Fe^{3+}. (C) The correlation between wavelength and the log concentration of Fe^{3+}.

Video file S1 (SI)). Furthermore, it is worth noting that the colors of the patterned PCS were almost colorless until the target concentration was below 50 ng ml^{-1}, which demonstrated that Fe^{3+} ions can strongly inhibit the activity of T-AgNPrs. In addition, it can also be observed in the inset of Fig. 5B that the value of RGB-based absorbance exhibits a good linear correlation with the concentration of Fe^{3+} over the linear range from 50 ng ml^{-1} to 1 μg ml^{-1}. The regression equation was $Abs_B = 0.5776C_{(Fe^{3+})} + 0.0249$, with appropriate linearity (R^2 value 0.9942).

The low limit of quantification (LLOQ) and sensitivity for Fe^{3+} in the proposed DES-PCS were calculated to be 50 ng ml^{-1} and 0.577 μg ml^{-1}, respectively. The results demonstrated that this DES-PCS is suitable for monitoring low concentrations of Fe^{3+} in environmental samples. The reproducibility and stability of DES-PCS were good since similar results were achieved for the three replicate analyses. Fig. 5C illustrates the relationship between Fe^{3+} concentration and wavelength. The chart indicates that as the concentration of Fe^{3+} ions increase, the wavelength decreases. In other words, at higher concentrations, Fe^{3+} ions absorb the light at shorter wavelengths. This behavior can be attributed to changes in the electronic structure of T-AgNPrs (optical probe) and interactions between Fe^{3+} ions and light. The shift in absorption wavelength corresponds to a change in color; when Fe^{3+} ions are present at higher concentrations, green light is absorbed more effectively, resulting in a shift toward yellow. The correlation between Fe^{3+} concentration and the wavelength of light absorbed in the PCS illustrates how the optical properties of these ions change as their concentration increases. This information can be valuable for gaining a deeper understanding of material behavior in PCSs. The data regarding the wavelength, average intensity of RGB, and the absorbance of developed DES-PCS at different concentrations of Fe(III) are presented in Table 3.

For a sensitivity study using the innovative DES-PCS for the determination of V(III), we systematically introduced various concentrations of V(III) into the sensing zones. Remarkably, we

Table 3 Wavelength, average intensity of RGB, and absorbance of developed DES-PCS of different concentrations of Fe(III)

Concentration of Fe^{3+} (μg ml^{-1})	Wavelength (nm)	Average color value [a]			RGB-based absorbance = −log [RGB/$R_0G_0B_0$]		
		A_R	A_G	A_B	Abs_R	Abs_G	Abs_B
Blank	601	219	208	198	0.0000	0.0000	0.0000
0.001	601	207	200	193	0.0245	0.0170	0.0111
0.005	601	208	200	192	0.0224	0.0170	0.0134
0.01	601	199	192	192	0.0416	0.0348	0.0134
0.05	594	218	210	192	0.0020	−0.0042	0.0134
0.1	591	213	205	176	0.0121	0.0063	0.0512
0.2	589	213	205	165	0.0121	0.0063	0.0792
0.4	588	215	204	131	0.0080	0.0084	0.1794
0.6	587	212	197	96	0.0141	0.0236	0.3144
0.8	587	213	194	70	0.0121	0.0303	0.4516
1	586	218	199	55	0.0020	0.0192	0.5563

[a] Data was shown in the mean with 3 times testing.

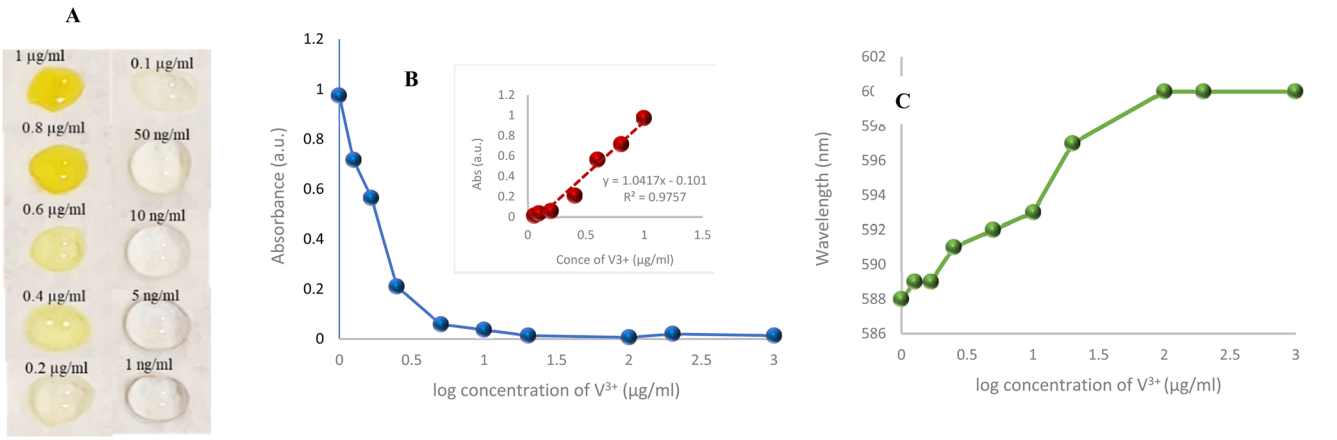

Fig. 6 Colorimetric results for V^{3+} determination using DES-PCD. (A) Images for the PCD displayed different V^{3+} amounts. (B) The calibration curve indicated the correlation between the value of RGB-based absorbance and the concentration of V^{3+}. (C) The correlation between wavelength and the log concentration of V^{3+}.

observed a distinct gold color change at concentrations of 1, 0.8, 0.6, 0.4, and 0.2 μg ml^{-1} of V^{3+} after a thorough 120 minutes incubation. In lower concentrations remained colorless throughout this period (see Video file S1, SI). These compelling results highlight the PCS's ability to effectively detect vanadium ions at higher concentrations, despite limitations at lower levels. Fig. 6B illustrates how different concentrations of V^{3+} influence the RGB-based absorbance, showing a significant increase in absorbance with rising V^{3+} concentrations. This demonstrates the robust potential of an engineered chemosensor for vanadium detection. The relationship between V^{3+}concentration and RGB-based absorbance is impressively linear within the range of 50 ng ml^{-1} to 1 μg ml^{-1}. This relationship is described by the regression equation: $Abs_B = 1.0417C_{(V^{3+})} - 0.101$, with a remarkable R^2 of 0.9757 (Fig. 6B). With an LLOQ set at 0.05 μg $ml^{-1}$and a sensitivity of 1.04 μg ml^{-1}, this method is highly suitable for monitoring low levels of V^{3+} in environmental samples. The relationship between the wavelength of the (DES/V^{3+}-T-AgNPrs) complex and the log concentration of V^{3+} ions, ranging from 1 ng ml^{-1} to 1 μg ml^{-1}, is plotted in Fig. 6C. It shows an inverse relationship between V^{3+} concentration and the wavelength of light absorbed; at lower concentrations (<0.05 μg ml^{-1}), the wavelength remains constant Table S2 (SI). Specifically, as V^{3+} concentration increases, the energy of the absorbed light increases, resulting in a shorter wavelength. At higher concentrations, optical interference phenomena may occur, possibly due to ion aggregation and changes in optical behavior. Overall, this inverse relationship highlights changes in the electronic structure and optical interactions driven by the increasing number of ions and environmental factors such as DES. This enhances our understanding of the optical properties of these chemical complexes on DES-PCS.

The chemosensing protocol for the determination of cobalt ion by engineered PCS was conducted as previously described. A standard Co(II) solution, with concentrations ranging from 50 ng ml^{-1} to 1 μg ml^{-1}, was applied to the sample zone of the PCS. The PCSs were then incubated at room temperature for 120

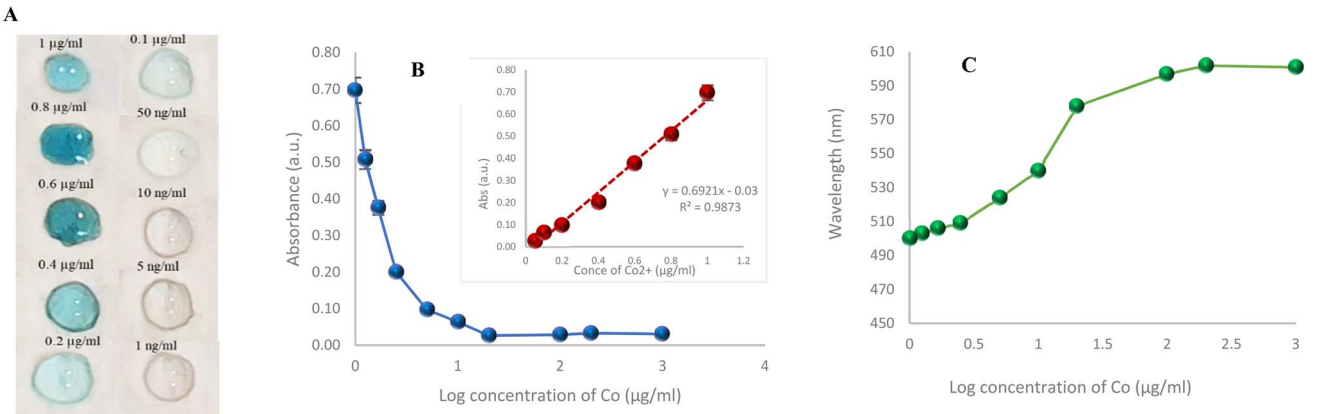

Fig. 7 Colorimetric results for Co^{2+} determination using DES-PCS. (A) Images for the PCS displayed different Co^{2+} amounts. (B) The calibration curve indicated the correlation between the value of RGB-based absorbance and the concentration of Co^{2+}. (C) The correlation between wavelength and the log concentration of Co^{2+}.

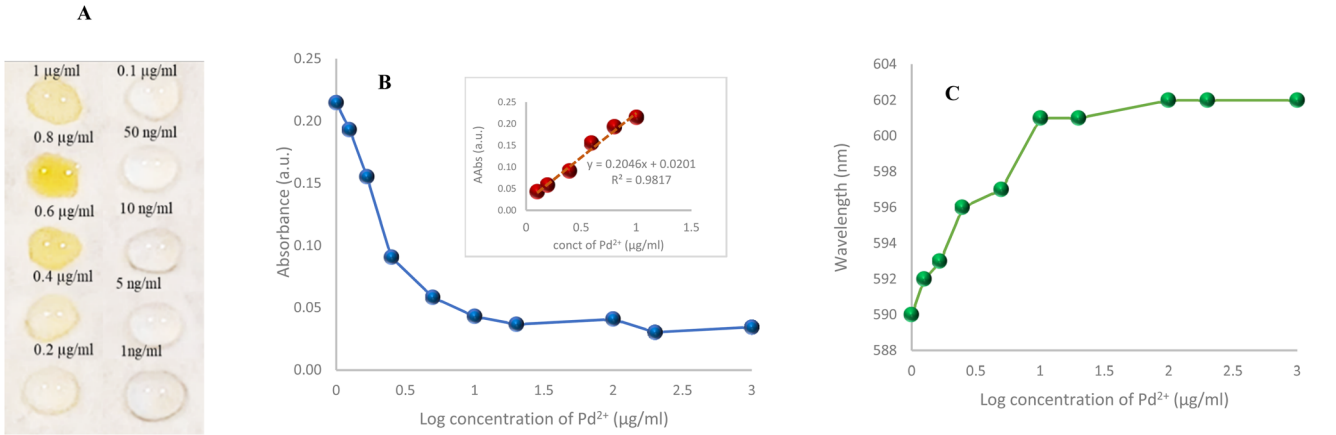

Fig. 8 Colorimetric results for Pd^{2+} determination using DES-PCS. (A) Images for the PCS displayed different Co^{2+} amounts. (B) The calibration curve indicated the correlation between the value of RGB-based absorbance and the concentration of Pd^{2+}. (C) The correlation between wavelength and the log concentration of Pd^{2+}.

minutes, allowing the reaction to reach completion. During this time, the T-AgNPrs that stabilized on the surface of PCS as an optical probe interacted with various concentrations of Co(II) in the presence of DES. Remarkably, as the incubation period for the DES/T-AgNPrs-Co^{2+} complex extended, the color transformed from vanilla (RGB: 243, 231, 180) at the beginning to a striking blue (RGB: 132, 181, 188) after 120 minutes (Fig. 7A). This notable color change not only underscores the selectivity of the probe but also demonstrates that higher concentrations of Co^{2+} (exceeding 50 ng ml^{-1}) lead to a more intense color complex, reinforcing the effectiveness of this method (Table S3 (SI)).

The sensitivity of the proposed PCS was investigated in the presence of various concentrations of Co^{2+}, as shown in Fig. 7. An excellent linearity was observed for the *R* channel in the concentration range of 50 ng ml^{-1} to 1 µg ml^{-1}, giving a regression equation of $Abs_R = 0.6921\times_{(Co^{2+})} - 0.03$ (Fig. 7B), with a correlation coefficient (R^2) of 0.9873. The LLOQ and sensitivity for Co^{2+} in the proposed PCS were calculated to be 50 ng ml^{-1} and 0.69 µg ml^{-1}, respectively. Wavelength can be influenced by the concentration of ions in the PCS system. Fig. 7C illustrates that as the concentration of Co^{2+} ions increase, the wavelength of light absorbed by the PCS system decreases due to changes in electronic transitions and concentration effects. This relationship is crucial for applications in sensing and material characterization. The change in absorption wavelength can also lead to observable color changes in the PCS, which can be used for qualitative analysis.

In a case of chemosensing of palladium, different concentrations (1, 0.8, 0.6, 0.4, 0,2, 0.1 µg ml^{-1}, 50, 10, 5, and 1 ng ml^{-1}) were added to detection zones of PCS, followed by the addition of 5 µL of freshly prepared T-AgNPrs into all wells. After 30 minutes of reaction time, the higher concentration of Pd^{2+} had undergone a color change to yellow (crayola) (RGB: 243, 225, 114). Almost 60 minutes later, the concentrations of 1, 0.8, 0.6, 0.4, and 0.2 µg ml^{-1} of Pd^{2+} were metallic gold RGB: in color, and the other concentrations were colorless (Fig. 8A). A calibration curve was established to accurately relate Pd^{2+} concentration to RGB-based absorbance of chemosensor, defined by the equation $Abs_B = 0.2046C_{(Pd^{2+})} + 0.0201$. The results exhibit impressive linearity, reflected in an R^2 value of 0.9817 (see Fig. 8B). This strong correlation confirms that the intensity of the color change is directly proportional to the high concentration of the analyte, underscoring the reliability of this method for the sensitive determination of Pd(II) in concentrations as high as 0.2 µg ml^{-1}. The LLOQ for Pd^{2+} has been determined to be 0.2 µg ml^{-1}, with a linear range extending from 0.2 to 1 µg ml^{-1}. Notably, the sensitivity of the method using the DES-PCS system is also recorded at 0.2 µg ml^{-1}, highlighting its effectiveness for precise measurements Table S4 (SI).

The relation between the wavelength of the color complex and the concentration of Pd^{2+} ions, ranging from 1 ng ml^{-1} to 1

Table 4 Analytical parameters of Fe(III), V(III), Co(II), and Pd(II) based on the DES-PCS

Analytical parameters	Fe(III)	V(III)	Co(II)	Pd(II)
Linear range (µg ml^{-1})	50 ng ml^{-1} – 1 µg ml^{-1}	50 ng ml^{-1} – 1 µg ml^{-1}	50 ng ml^{-1} – 1 µg ml^{-1}	0.2 µg ml^{-1} – 1 µg ml^{-1}
R value	0.9942	0.9757	0.9873	0.9817
LLOQ[a]	50 ng ml^{-1}	50 ng ml^{-1}	50 ng ml^{-1}	0.2 µg ml^{-1}
Sensitivity[b]	0.577 µg ml^{-1}	1.041 µg ml^{-1}	0.69 µg ml^{-1}	0.204

[a] Lowest limitation of quantification. [b] sensitivity defined in this way is equal to the slope of the analytical calibration curve.

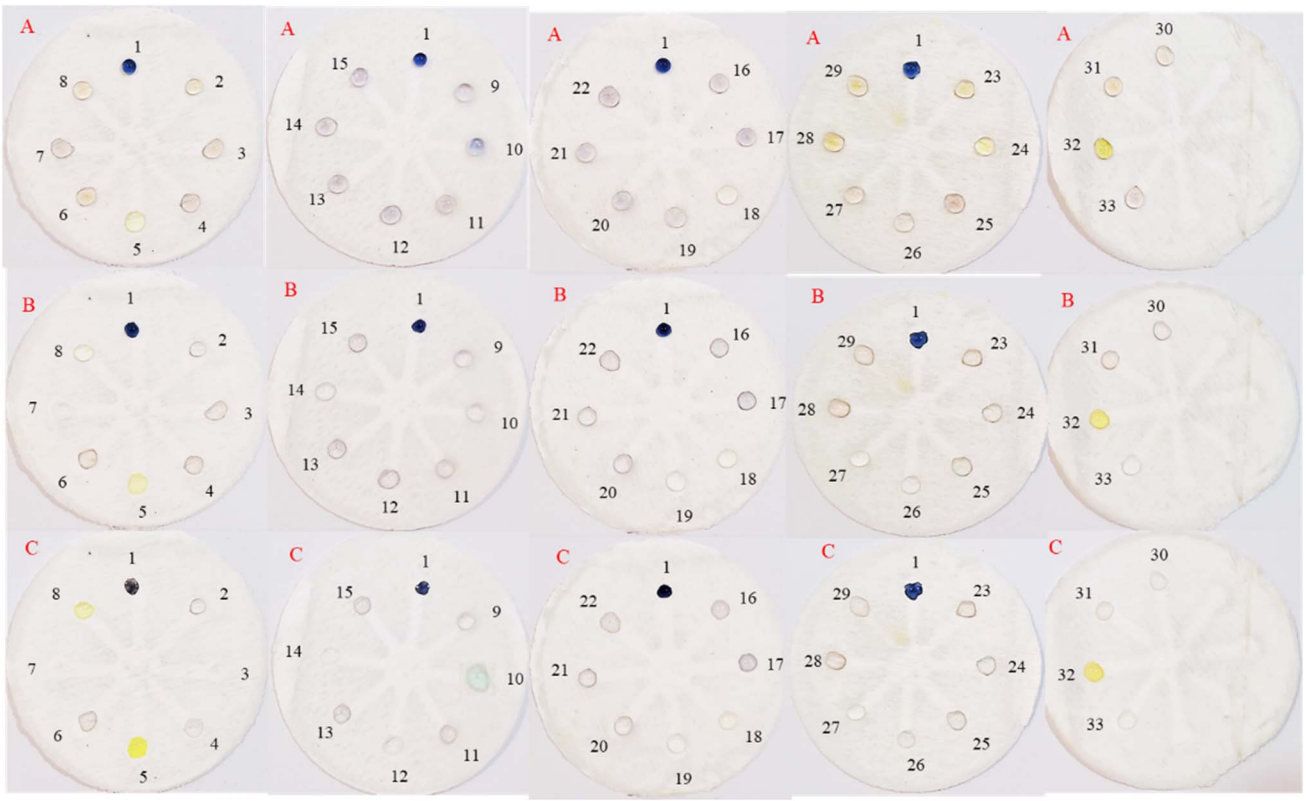

Fig. 9 Selectivity of DES-PCS for detection of Fe^{3+}, V^{3+}, Co^{2+}, and Pd^{2+}.The photograph shows DES-PCS colorimetric response for individual identification of various control ions and Fe^{3+}, V^{3+}, Co^{2+}, and Pd^{2+} at different reaction times (A) after 5 minutes, (B) after 30 minutes, and (C) after 60 minutes: (1) T-AgNPrs, (2) T-AgNPrs + DES, (3) T-AgNPrs + DES + As^{5+}, (4) T-AgNPrs + DES + B^{+}, (5) T-AgNPrs + DES + Fe^{3+}, (6) T-AgNPrs + DES + Ca^{2+}, (7) T-AgNPrs + DES + Te^{4+}, (8) T-AgNPrs + DES + V^{3+}, (9) T-AgNPrs + DES + Sr^{2+}, (10) T-AgNPrs + DES + W^{6+}, (11) T-AgNPrs + DES + Co^{2+}, (12) T-AgNPrs + DES + Zr^{4+}, (13) T-AgNPrs + DES + Na^{+}, (14) T-AgNPrs + DES + Mo^{6+}, (15) T-AgNPrs + DES + Al^{3+}, (16) T-AgNPrs + DES + Ba^{2+}, (17) T-AgNPrs + DES + Cr^{3+}, (18) T-AgNPrs + DES + Pt^{4+}, (19) T-AgNPrs + DES + Bi^{3+}, (20) T-AgNPrs + DES + Sn^{2+}, (21) T-AgNPrs + DES + Mn^{2+}, (22) T-AgNPrs + DES + Pb^{2+}, (23) T-AgNPrs + DES + Ni^{2+}, (24) T-AgNPrs + DES + Cs^{+}, (25) T-AgNPrs + DES + Si^{4+}, (26) T-AgNPrs + DES + Hg^{2+}, (27) T-AgNPrs + DES + Se^{4+}, (28) T-AgNPrs + DES + k^{+}, (29) T-AgNPrs + DES + Li^{+}, (30) T-AgNPrs + DES + Zn^{2+}, (31) T-AgNPrs + DES + Mg^{2+}, (32) T-AgNPrs + DES + Pd^{2+}, (33) T-AgNPrs + DES + Cu^{2+} with volume ratio (1 : 1 : 1).

μg ml^{-1}, is depicted in Fig. 8C. This graph illustrates a compelling inverse relationship at high concentrations (>0.2 μg ml^{-1}). As the concentration of Pd^{2+} ions rise, the energy of the absorbed light correspondingly increases, resulting in a shorter wavelength. This finding emphasizes the significant impact of Pd^{2+} concentration on light absorption, highlighting its importance in analytical applications.

The analytical performances for all four ion targets are summarized in Table 4. It can be seen that a sufficiently low detection limit could be obtained for Fe^{3+}, V^{3+}, Cd^{2+}, and Pd^{2+}detection. Moreover, this multiplex system enables sensitive and selective detection of metal ion targets simultaneously in a single device, simplifying the analysis compared to traditional diagnostics.

3.5 Selectivity of DES-PCSs for detection Fe^{3+}, V^{3+}, Co^{2+}, and Pd^{2+} ions

The specificity of this new system was examined by observing the response to a various of metallic ions (As^{3+}, B^{3+}, Fe^{3+}, Ca^{2+}, Te^{4+}, V^{3+}, Sr^{2+}, W^{6+}, Co^{2+}, Zr^{4+}, Na^{+}, Mo^{6+}, Al^{3+}, Ba^{2+}, Cr^{3+}, Pt^{4+}, Bi^{3+}, Sn^{2+}, Mn^{2+}, Pb^{2+}, Ni^{2+}, Cs^{+}, Si^{4+}, Hg^{2+}, Se^{4+}, K^{+}, Li^{+}, Zn^{2+}, Mg^{2+}, Pd^{2+}, and Cu^{2+}) under the same experimental conditions used for Fe^{3+}, V^{3+}, Co^{2+}, and Pd^{2+} sensing. To achieve this, the final concentrations of Fe^{3+}, V^{3+}, Co^{2+}, Pd^{2+} ions, and other ions were adjusted to 1 μg ml^{-1} and individually dropped onto the sensing zone. Immediately afterward, DES mixed with T-AgNPrs (in a 1 : 1 V/V ratio) was immobilized onto them (see Fig. 9 and Video file S2 (SI)). By comparing the color intensities of the paper chips for different metal ions, it was observed that all control ions exerted inhibitory effects on the T-AgNPrs in the presence of the DES, leading to the formation of colorless areas. However, the metal ions Fe^{3+}, V^{3+}, Co^{2+}, and Pd^{2+} ions resulted in the most noticeable color changes, specifically in detection zones 5, 8,10, and 32 of PCSs, respectively. These findings demonstrate that the method provides excellent specificity and selectivity for detecting Fe^{3+}, V^{3+}, Co^{2+}, and Pd^{2+} among 31 different metal ions. The PCSs decorated with T-AgNPrs, which selectively target ions in the presence of DES, showed high color intensity and uniformity, making them suitable for field and on-site environmental monitoring.

The specificity and competitive properties of PCS were tested by observing the reaction of metallic ions with T-AgNPrs in the

absence of DES. To achieve this, T-AgNPrs is dropped onto the detection zones as an optical probe. Immediately afterward, the cation ions were individually dropped onto the detection zone (in a 1 : 1 V/V ratio). These observations were recorded immediately after the reaction (5 min) and again at 30 and 60 minutes intervals (see Fig. S1). When comparing the color intensities of PCS with various metal ions, it was found that all of the tested ions had inhibitory effects on the T-AgNPrs, resulting in a colorless complex.

3.6 Stability of the sensing system

The stabilization of reagents on the paper substrate, which amounts to the stability of the PADs themselves during storage. When we need chemical analyses out of the laboratory, the PADs must exhibit stability during transport and storage. To explore the possibility of producing on-site diagnostic kits with PCSs, the stability of the designed DES-PCS was assessed over a period of time. For this purpose, the PADs were functionalized by dropping target ions, optical probe, and DES, then stored at ambient temperature (25 °C ± 2 °C) for 60 days. The *R* value as a function of the stability sensing system is shown in Fig. S2 (SI) for the cobalt ion. These results indicate that more than 90% of the initial response was retained without significant loss of functionality, confirming the stability of the fabricated colorimetric sensor.

In this study, spot-based colorimetric PADs do not experience color complex vaporization due to an element known as a DES. In contrast, without a DES, the color complex tends to vaporize from the paper surface. Additionally, in the presence of DES, a significant increase in the stability of the sensing system was observed. The color complex formed in the DES remained stable for several days without drying and vaporization.

3.7 Detection of Fe^{3+}, V^{3+}, Co^{2+}, and Pd^{2+} ions in real samples

Based on sensitivity and selectivity studies, the feasibility of using the DES-PCS for ion sensing in urine samples was assessed. Urine samples were collected from healthy volunteers with no history of drug use. The colorimetric sensing was performed by engineered PCS. The signal intensities of Fe^{3+}, V^{3+}, Co^{2+}, and Pd^{2+} in human urine samples were compared to those from standard solutions of these ions at concentrations of 1 $ng.ml^{-1}$ to 1 $\mu g.ml^{-1}$, with experiments performed in triplicate. Since real samples can be complex, the standard addition method was employed for ion detection. For this, various concentrations of each ion (1 ng ml^{-1} to 1 μg ml^{-1}) were prepared in the DESs and mixed with human urine samples at a 1 : 1 volume ratio. These mixtures and the chemical probe were then applied to the DES-PCS in equal parts, and their interaction was evaluated using the colorimetric method. Calibration curves were obtained by plotting absorbance, derived from the RGB values, against the different concentrations of the analyte (Fig. S3A–D (SI)) in the real sample. The correlation coefficients were obtained as 0.9465, 0.9833, 0.9801, and 0.9876 for Fe^{3+}, V^{3+}, Co^{2+}, and Pd^{2+}, respectively.

The selectivity of the DES-PCS was utilized to identify different ions in human urine samples. Results are presented in Fig. S4 (SI) and (Video file S3) at three time points after incubation times of 5, 30, and 60 minutes. The color changes from the human urine samples closely resembled those of the standard samples, as seen in Fig. S4 (SI), which indicated that this new sensing platform would be suitable for the assay of trace amounts of Fe^{3+}, V^{3+}, Co^{2+}, and Pd^{2+} in real samples.

The signal intensities of Fe^{3+}, V^{3+}, Co^{2+}, and Pd^{2+} in spiked urine samples were compared to those obtained from standard solutions of Fe^{3+}, V^{3+}, Co^{2+}, and Pd^{2+} at concentrations of 0.2, 0.6, and 1 μg ml^{-1}. The analyses were performed in triplicate. Fig. S5 (SI) demonstrates that the response values from the human urine samples closely matched the results from the standard solutions. This correlation indicates that the new sensing platform is suitable for detecting trace levels of Fe^{3+}, V^{3+}, Co^{2+}, and Pd^{2+} in real samples.

The color intensities obtained from the human urine samples almost matched those of the standard samples. Although the urine samples contained a significant amount of various chemical compounds, both the standard and urine samples formed metal complexes in their designated detection zones without noticeable cross-reactions. From this comparison, we confirmed that the presence of various chemical compounds in the urine samples did not significantly affect overall reaction efficiency and sensitivity. Heavy metal ions were detected in urine samples without any pre-treatment, and we evaluated the potential bias from contaminants and cross-reactive chemicals. From untreated urine samples, we confirmed that other analytes present in the real sample did not reduce the reaction efficiency, sensitivity, or specificity of the PCS.

4 Conclusion

A portable DES-PCS that uses T-AgNPrs as an optical probe was developed for chemosensing Fe^{3+}, V^{3+}, Co^{2+}, and Pd^{2+} ions *via* a colorimetric assay. The PCS device was designed to be easy to use, cost-effective, and simple to manufacture, eliminating the need for a sterile environment or specialized equipment. To achieve this, the reaction of the analyte with T-AgNPrs in the presence of DES (DES/ion-T-AgNPrs) was utilized to produce a colored product on the PADs. The device is integrated with a smartphone for a digital readout of color intensity. Therefore, a novel approach for on-site monitoring of Fe^{3+}, V^{3+}, Co^{2+}, and Pd^{2+} ions was proposed by combining a DES with PADs decorated with T-AgNPrs. The proposed PCS shows high sensitivity for detecting these ions, with a low LLOD (50 ng ml^{-1} for Fe(III), V(III), Co(II), and 0.2 μg ml^{-1} for Pd(II)). Results indicate that the new sensing platform is suitable for detecting trace levels of Fe^{3+}, V^{3+}, Co^{2+}, and Pd^{2+} in real samples. Control experiments confirm that DES alone does not produce significant color changes with analytes, underscoring the crucial role of T-AgNPrs in mediating the sensor response. It is important to point out that, DES acts primarily as a stabilizer and aggregation inducer, while T-AgNPrs mediate the selective color response. This work represents a significant advancement in

PCS technology, addressing critical limitations of existing platforms while remaining simple and affordable. Testing in human urine samples confirmed the device's effectiveness for cations under optimal conditions.

Due to its low reagent and analyte consumption (μL scale), this paper-based platform offers advantages such as low cost, convenience, and near real-time results. It holds significant promise as a new tool for field measurement of metal ions, especially in underdeveloped countries, and this study also proposed an effective stabilizer to enhance the practicality of PADs for on-site monitoring of various analytes in real samples.

Conflicts of interest

There are no conflicts to declare.

Data availability

The authors declare that the data supporting the findings of this study are included within the article. Any data supporting this article have been included as part of the supplementary information (SI). Supplementary information: Table S1: molar ratio, density, viscosity, conductivity, and structure of selected DESs. Table S2: wavelength, average intensity of RGB, and absorbance of developed DES-PCS of different concentrations of V(III). Table S3: wavelength, average intensity of RGB, and absorbance of developed DES-PCS of different concentrations of Co(II). Table S4: wavelength, average intensity of RGB, and absorbance of developed DES-PCS of different concentrations of Pd(II). Fig. S1: the photograph shows PCS colorimetric response decorated with T-AgNPrs for individual identification of various control ions in the absence of DES at different reaction times (A) after 5 minutes, (B) after 30 minutes, and (C) after 60 minutes: T-AgNPrs, (1) T-AgNPrs + As^{5+}, (2) T-AgNPrs + B^{+}, (3) T-AgNPrs + Fe^{3+}, (4) T-AgNPrs + Ca^{2+}, (5) T-AgNPrs + Te^{4+}, (6) T-AgNPrs + V^{3+},(7) T-AgNPrs + Sr^{2+}, (8) T-AgNPrs + W^{6+}, (9) T-AgNPrs + Co^{2+}, (10) T-AgNPrs + Zr^{4+}, (11) T-AgNPrs + Na^{+}, (12) T-AgNPrs + Mo^{6+}, (13) T-AgNPrs + Al^{3+}, (14) T-AgNPrs + Ba^{2+}, (15) T-AgNPrs + Cr^{3+}, (16) T-AgNPrs + Pt^{4+}, (17) T-AgNPrs + Bi^{3+}, (18) T-AgNPrs + Sn^{2+}, (19) T-AgNPrs + Mn^{2+}, (20) T-AgNPrs + Pb^{2+}, (21) T-AgNPrs + Ni^{2+}, (22) T-AgNPrs + Cs^{+}, (23) T-AgNPrs + Si^{4+}, (24) T-AgNPrs + Hg^{2+}, (25) T-AgNPrs + Se^{4+}, (26) T-AgNPrs + k^{+}, (27) T-AgNPrs + Li^{+}, (28) T-AgNPrs + Zn^{2+}, (29) T-AgNPrs + Mg^{2+}, (30) T-AgNPrs + Pd^{2+}, (31) T-AgNPrs + Cu^{2+} with volume ratio (1 : 1 : 1). Fig. S2: the stability of the DES-PCS for Co^{2+} detection. The PADs were stored at room temperature (25 °C ± 2 °C) for 60 days. Fig. S3: the calibration curve indicated the correlation between the value of RGB-based absorbance and the different concentrations of (A) Fe(III), (B) V(III), (C) Co(II), and (D) Pd(II) ions. Fig. S4: the digital images of DES-PCS colorimetric response for individual identification of various ions human urine samples by the Spike method at three distinct incubation reaction times (A) after 5 minutes, (B) after 30 minutes, and (C) after 60 minutes: (1) T-AgNPrs + DES, (2) T-AgNPrs + DES + As^{5+}, (3) T-AgNPrs + DES + B^{+}, (4) T-AgNPrs + DES+ Fe^{3+}, (5) T-AgNPrs + DES + Ca^{2+}, (6) T-AgNPrs + DES + Te^{4+}, (7) T-AgNPrs + DES + V^{3+}, (8) T-AgNPrs + DES + Sr^{2+}, (9) T-AgNPrs + DES + W^{6+}, (10) T-AgNPrs + DES + Co^{2+}, (11) T-AgNPrs + DES + Zr^{4+}, (12) T-AgNPrs + DES + Na^{+}, (13) T-AgNPrs + DES + Mo^{6+}, (14) T-AgNPrs + DES + Al^{3+}, (15) T-AgNPrs + DES + Ba^{2+}, (16) T-AgNPrs + DES + Cr^{3+}, (17) T-AgNPrs + DES + Pt^{4+}, (18) T-AgNPrs + DES + Bi^{3+}, (19) T-AgNPrs + DES + Sn^{2+}, (20) T-AgNPrs + DES + Mn^{2+}, (21) T-AgNPrs + DES + Pb^{2+}, (22) T-AgNPrs + DES + Ni^{2+}, (23) T-AgNPrs + DES + Cs^{+}, (24) T-AgNPrs + DES + Si^{4+}, (25) T-AgNPrs + DES + Hg^{2+}, (26) T-AgNPrs + DES + Se^{4+}, (27) T-AgNPrs + DES + k^{+}, (28) T-AgNPrs + DES + Li^{+}, (29) T-AgNPrs + DES + Zn^{2+}, (30) T-AgNPrs + DES + Mg^{2+}, (31) T-AgNPrs + DES + Pd^{2+}, (32) T-AgNPrs + DES + Cu^{2+} with volume ratio (1 : 1 : 1). Fig. S5: real samples colorimetric assay by DES-PCS with 0.2, 0.6, and 1 μg ml^{-1} standard solution (black) and spiked urine samples analysis (red) for (A) Fe^{3+}, (B) V^{3+}, (C) Co^{2+}, and (D) Pd^{2+} ions. See DOI: https://doi.org/10.1039/d5ra07032e.

Acknowledgements

The findings of this study were derived from the PhD dissertation (3400808) submitted to Esfahan University of Medical Sciences. We would like to express our gratitude to Tabriz University of Medical Sciences, especially the Pharmaceutical Analysis Research Center in Tabriz, Iran (77564), for their instrumental assistance and the resources they provided during this research.

References

1 J. G. Paithankar, S. Saini, S. Dwivedi, A. Sharma and D. K. Chowdhuri, Heavy metal associated health hazards: An interplay of oxidative stress and signal transduction, *Chemosphere*, 2021, **262**, 128350.

2 C. Zamora-Ledezma, D. Negrete-Bolagay, F. Figueroa, E. Zamora-Ledezma, M. Ni, F. Alexis, *et al.*, Heavy metal water pollution: A fresh look about hazards, novel and conventional remediation methods, *Environ. Technol. Innovation*, 2021, **22**, 101504.

3 S. Mitra, A. J. Chakraborty, A. M. Tareq, T. B. Emran, F. Nainu, A. Khusro, *et al.*, Impact of heavy metals on the environment and human health: Novel therapeutic insights to counter the toxicity, *J. King Saud Univ., Sci.*, 2022, **34**(3), 101865.

4 S. Malik, J. Singh, A. Umar, A. A. Ibrahim and S. Baskoutas, Smartphone-integrated paper sensor strips for rapid and on-site detection of heavy metal ions in environmental water samples, *J. Photochem. Photobiol., A*, 2025, 116675.

5 G. Khayatian, M. Moradi and S. Hassanpoor, MnO2/3MgO nanocomposite for preconcentration and determination of trace copper and lead in food and water by flame atomic absorption spectrometry, *J. Anal. Chem.*, 2018, **73**(5), 470–478.

6 A. Mourya, B. Mazumdar and S. K. Sinha, Determination and quantification of heavy metal ion by electrochemical method, *J. Environ. Chem. Eng.*, 2019, **7**(6), 103459.

7 R. Ding, Y. H. Cheong, A. Ahamed and G. Lisak, in. *Heavy Metals Detection with Paper-Based Electrochemical Sensors*, ACS Publications, 2021.

8 S. R. Khan, B. Sharma, P. A. Chawla and R. Bhatia, Inductively coupled plasma optical emission spectrometry (ICP-OES): a powerful analytical technique for elemental analysis, *Food Anal. Methods*, 2022, **15**(3), 666–688.
9 N. Limchoowong, P. Sricharoen, S. Techawongstien and S. Chanthai, Using bio-dispersive solution of chitosan for green dispersive liquid–liquid microextraction of trace amounts of Cu (II) in edible oils prior to analysis by ICP–OES, *Food Chem.*, 2017, **230**, 398–404.
10 W. Chen, Y. Yang, K. Fu, D. Zhang and Z. Wang, Progress in ICP-MS analysis of minerals and heavy metals in traditional medicine, *Front. Pharmacol.*, 2022, **13**, 891273.
11 S. Echioda, A. O. Ogunieye, S. Salisu, A. A. Abdulrasheed, I. Chindo and A. Kolo, UV-Vis spectrophotometric determination of selected heavy metals (Pb, Cr, Cd and As) in environmental, water and biological samples with synthesized glutaraldehyde phenyl hydrazone as the chromogenic reagent, *Eur. J. Adv. Chem.*, 2021, **2**(3), 1–5.
12 A. K. Yetisen, M. S. Akram and C. R. Lowe, based microfluidic point-of-care diagnostic devices, *Lab Chip*, 2013, **13**(12), 2210–2251.
13 T. Akyazi, L. Basabe-Desmonts and F. Benito-Lopez, Review on microfluidic paper-based analytical devices towards commercialisation, *Anal. Chim. Acta*, 2018, **1001**, 1–17.
14 P. Aryal and C. S. Henry, Advancements and challenges in microfluidic paper-based analytical devices: design, manufacturing, sustainability, and field applications, *Front. Lab Chip Technol.*, 2024, **3**, 1467423.
15 J. P. Devadhasan and J. Kim, A chemically functionalized paper-based microfluidic platform for multiplex heavy metal detection, *Sens. Actuators, B*, 2018, **273**, 18–24.
16 H. Sharifi, J. Tashkhourian and B. Hemmateenejad, Identification and determination of multiple heavy metal ions using a miniaturized paper-based optical device, *Sens. Actuators, B*, 2022, **359**, 131551.
17 H. A. Silva-Neto, I. V. Arantes, A. L. Ferreira, G. H. do Nascimento, G. N. Meloni, W. R. de Araujo, *et al.*, Recent advances on paper-based microfluidic devices for bioanalysis, *TrAC, Trends Anal. Chem.*, 2023, **158**, 116893.
18 T. Pinheiro, A. R. Cardoso, C. E. Sousa, A. C. Marques, A. P. Tavares, A. M. Matos, *et al.*, based biosensors for COVID-19: a review of innovative tools for controlling the pandemic, *ACS Omega*, 2021, **6**(44), 29268–29290.
19 P. Aryal, C. Hefner, B. Martinez and C. S. Henry, Microfluidics in environmental analysis: advancements, challenges, and future prospects for rapid and efficient monitoring, *Lab Chip*, 2024, **24**(5), 1175–1206.
20 A. Du, Z. Lu and L. Hua, Decentralized food safety and authentication on cellulose paper-based analytical platform: A review, *Compr. Rev. Food Sci. Food Saf.*, 2024, **23**(5), e13421.
21 W. A. Ameku, W. R. de Araujo, C. J. Rangel, R. A. Ando and T. R. Paixao, Gold nanoparticle paper-based dual-detection device for forensics applications, *ACS Appl. Nano Mater.*, 2019, **2**(9), 5460–5468.
22 S. Smith, J. G. Korvink, D. Mager and K. Land, The potential of paper-based diagnostics to meet the ASSURED criteria, *RSC Adv.*, 2018, **8**(59), 34012–34034.
23 K. Yamada, H. Shibata, K. Suzuki and D. Citterio, Toward practical application of paper-based microfluidics for medical diagnostics: state-of-the-art and challenges, *Lab Chip*, 2017, **17**(7), 1206–1249.
24 G. G. Morbioli, T. Mazzu-Nascimento, A. M. Stockton and E. Carrilho, Technical aspects and challenges of colorimetric detection with microfluidic paper-based analytical devices (μPADs)-A review, *Anal. Chim. Acta*, 2017, **970**, 1–22.
25 W. Tan, L. Zhang, P. Jarujamrus, J. C. Doery and W. Shen, Improvement strategies on colorimetric performance and practical applications of Paper-based analytical devices, *Microchem. J.*, 2022, **180**, 107562.
26 J.-S. Wi, J. D. Kim, W. Lee, H. Choi, M. Kwak, J. Song, *et al.*, Inkjet-printable nanoporous Ag disk arrays enabling coffee-ring effect-driven analyte enrichment towards practical SERS Applications, *Int. J. Precis. Eng. Manuf.–Green Technol.*, 2022, **9**(2), 421–429.
27 C. Grazioli, G. Faura, N. Dossi, R. Toniolo, F. Tubaro, F. Terzi, *et al.*, A colorimetric paper-based smart label soaked with a deep-eutectic solvent for the detection of malondialdehyde, *Sens. Actuators, B*, 2021, **329**, 129174.
28 H. Sharifi, J. Tashkhourian and B. Hemmateenejad, A 3D origami paper-based analytical device combined with PVC membrane for colorimetric assay of heavy metal ions: Application to determination of Cu (II) in water samples, *Anal. Chim. Acta*, 2020, **1126**, 114–123.
29 W. I. S. Galpothdeniya, K. S. McCarter, S. L. De Rooy, B. P. Regmi, S. Das, F. Hasan, *et al.*, Ionic liquid-based optoelectronic sensor arrays for chemical detection, *RSC Adv.*, 2014, **4**(14), 7225–7234.
30 S. Chen, Y. Dong, J. Sun, P. Gu, J. Wang and S. Zhang, Ionic liquids membranes for liquid separation: status and challenges, *Green Chem.*, 2023, **25**(15), 5813–5835.
31 C. Florindo, F. Lima, B. D. Ribeiro and I. M. Marrucho, Deep eutectic solvents: overcoming 21st century challenges, *Curr. Opin. Green Sustainable Chem.*, 2019, **18**, 31–36.
32 A. Prabhune and R. Dey, Green and sustainable solvents of the future: Deep eutectic solvents, *J. Mol. Liq.*, 2023, **379**, 121676.
33 E. L. Smith, A. P. Abbott and K. S. Ryder, Deep eutectic solvents (DESs) and their applications, *Chem. Rev.*, 2014, **114**(21), 11060–11082.
34 K. de Oliveira Vigier and J. García-Álvarez, Deep eutectic and low-melting mixtures, *Bio-Based Solvents*, 2017, **93**(14), 83–114.
35 J. Płotka-Wasylka, M. De la Guardia, V. Andruch and M. Vilková, Deep eutectic solvents *vs.* ionic liquids: Similarities and differences, *Microchem. J.*, 2020, **159**, 105539.
36 P. Janicka, M. Kaykhaii, J. Płotka-Wasylka and J. Gębicki, Supramolecular deep eutectic solvents and their applications, *Green Chem.*, 2022, **24**(13), 5035–5045.

37 B. B. Hansen, S. Spittle, B. Chen, D. Poe, Y. Zhang, J. M. Klein, *et al.*, Deep eutectic solvents: a review of fundamentals and applications, *Chem. Rev.*, 2020, **121**(3), 1232–1285.

38 M. B. S. Mr, V. S. K. Mr, M. Chaudhary and P. Singh, A mini review on synthesis, properties and applications of deep eutectic solvents, *J. Indian Chem. Soc.*, 2021, **98**(11), 100210.

39 T. El Achkar, H. Greige-Gerges and S. Fourmentin, Basics and properties of deep eutectic solvents: a review, *Environ. Chem. Lett.*, 2021, **19**(4), 3397–3408.

40 W. Alahmad, A. Sahragard and P. Varanusupakul, An overview of the recent developments of microfluidic paper-based analytical devices for the detection of chromium species, *Microchem. J.*, 2021, **170**, 106699.

41 J. Guo, G. Wang, J. Zou and Z. Lei, Chitosan modified cuprous oxide nanoparticles with specific oxidoreductase-like activity for rapid and sensitive colorimetric detection of Cr (VI), *Colloids Surf., A*, 2024, **686**, 133356.

42 K. Shrivas, B. Sahu, M. K. Deb, S. S. Thakur, S. Sahu, R. Kurrey, *et al.*, Colorimetric and paper-based detection of lead using PVA capped silver nanoparticles: experimental and theoretical approach, *Microchem. J.*, 2019, **150**, 104156.

43 Q. Liu, Y. Lin, J. Xiong, L. Wu, X. Hou, K. Xu, *et al.*, Disposable paper-based analytical device for visual speciation analysis of Ag(I) and silver nanoparticles (AgNPs), *Anal. Chem.*, 2019, **91**(5), 3359–3366.

44 K. Khachornsakkul, D. Phuengkasem, K. Palkuntod, W. Sangkharoek, O. Jamjumrus and W. Dungchai, A simple counting-based measurement for paper analytical devices and their application, *ACS Sens.*, 2022, **7**(7), 2093–2101.

45 D. Kumar and N. Kaur, Rigid anthraquinone based sensor for dual and differential colorimetric detection of Cu2+ and Ni2+ ions: mimicking different molecular logic systems, *Results Chem.*, 2022, **4**, 100563.

46 M. El-Maghrabey, S. Seino, N. Kishikawa and N. Kuroda, The Development of a Selective Colorimetric Sensor for Cu^{2+} and Zn^{2+} in Mineral Supplement with Application of a Smartphone Paper-Based Assay of Cu^{2+} in Water Samples, *Sensors*, 2024, **24**(23), 7844.

47 S. Muhammad-Aree and S. Teepoo, On-site detection of heavy metals in wastewater using a single paper strip integrated with a smartphone, *Anal. Bioanal. Chem.*, 2020, **412**(6), 1395–1405.

48 N. Idros and D. Chu, Triple-indicator-based multidimensional colorimetric sensing platform for heavy metal ion detections, *ACS Sens.*, 2018, **3**(9), 1756–1764.

49 X. Xiong, J. Zhang, Z. Wang, C. Liu, W. Xiao, J. Han, *et al.*, Simultaneous multiplexed detection of protein and metal ions by a colorimetric microfluidic paper-based analytical device, *BioChip J.*, 2020, **14**(4), 429–437.

50 J. Yue, Q. Lv, W. Wang and Q. Zhang, Quantum-dot-functionalized paper-based device for simultaneous visual detection of Cu (II), Mn (II), and Hg (II), *Talanta*, 2022, **5**, 100099.

51 R. Tayefeh-Rahimian, M. Rismanchian and M. Hasanzadeh, Plasmonic chemosensing of W(VI), Pd(II), Cr(III), and Cs(I) in deep eutectic solvent using silver nanoparticles: green solvent toward optical point-of-use quality testing, *RSC Adv.*, 2025, **15**, 28021.

52 A. Saadati, F. Farshchi, M. Hasanzadeh, Y. Liu and F. Seidi, Colorimetric and naked-eye detection of arsenic(iii) using a paper-based microfluidic device decorated with silver nanoparticles, *RSC Adv.*, 2022, **12**, 21836–21850.

53 T. S. Kuntzleman and E. C. Jacobson, Teaching Beer's law and absorption spectrophotometry with a smart phone: a substantially simplified protocol, *J. Chem. Educ.*, 2016, **93**(7), 1249–1252.

54 E. Evans, E. F. M. Gabriel, W. K. T. Coltro and C. D. Garcia, Rational selection of substrates to improve color intensity and uniformity on microfluidic paper-based analytical devices, *Analyst*, 2014, **139**(9), 2127–2132.

55 N. Sharma, T. Barstis and B. Giri, Advances in paper-analytical methods for pharmaceutical analysis, *Eur. J. Pharmacol.*, 2018, **111**, 46–56.